1994

The Importance Of Taper In Luminal Arterial Geometry: An In Vitro And In Vivo Analysis

Neil Francis MacLean

THE IMPORTANCE OF TAPER IN LUMINAL ARTERIAL GEOMETRY: AN *IN VITRO* AND *IN VIVO* ANALYSIS

by

Neil Francis MacLean

Department of Medical Biophysics

Submitted in partial fulfillment
of the requirements for the degree of
Doctor of Philosophy

Faculty of Graduate Studies
The University of Western Ontario
London, Ontario
August 1993

ISBN 0-315-90557-3

Canada

Abstract

Arterial diseases such as atherosclerosis and aneurysms occur in human arteries, and may be induced by local differences in hemodynamic or elastic forces. Both of these forces are tied to the geometry of the lumen. The goal of this study was to measure luminal cross-sectional area variation (area taper) in Y-bifurcations of muscular arteries (porcine renals) and elastic arteries (human aorto-iliac), and compare these bifurcations with data obtained previously on muscular human cerebral bifurcations. Flow accelerates as the arteries taper and decelerates as they flare. Separation zones develop with flaring.

The arteries were pressure-fixed, frozen and sliced at 10-40μm. Luminal area was measured digitally from the block face (this removed histological artifacts). Area taper, defined as the change in luminal area per unit length of artery, was calculated and found to be - 1.4mm (± 0.2 mm S.E.M.) (n=13) in the parent branch of the renal arterial bifurcations and -1.5mm ± 0.3mm (n=6) in the parent branch of human cerebral bifurcations. Negative area taper corresponded to an expansion. The maximum cross-sectional area was at the flow divider in both renal and cerebral bifurcations but not in the aorto-iliac bifurcation. The human aorto-iliac had three area tapers: -0.7 ± 0.1mm in the pre-apical region, +2.4 ± 0.7mm in the apical region and -1.1 ± 0.3 post-apically.

In vivo geometry of the human abdominal aorta was measured from aorto-grams and computed tomographic (CT) scans from patients with and without aneurysms. CT scans (n= 25) showed the aortic lumen to be circular. Aortograms of normal aortas (n=8) showed diameter tapers of +0.07 ± 0.02 proximal to the throat and -0.63 ± 0.06 proximal to the flow divider. Abdominal aortic aneurysms had three diameter tapers: -0.6 ± 0.2 proximal to the maximum aneurysm area (apex), +0.4 ± 0.1 distal to the apex and -0.6 ± 0.1 proximal to the flow divider.

The large tapers make measurements of area ratio reported previously prone

to error. Area taper is a more valid parameter to describe bifurcation geometry. Since tapers were not significantly different in porcine renal and human cerebral bifurcations, hemodynamic factors seem less likely than structural factors to explain why aneurysms develop at the apex of cerebral bifurcations.

Acknowledgements

The studies presented in this thesis would not have been possible without the help provided by the following individuals:

Dr. Roach: My friend and mentor who has taught me to believe in myself, and encouraged me to make my own decisions and mistakes. Thank you for the chance to prove myself.

My advisory committee: I am greatful for the help, wisdom and guidance provided by my advisory committee: Drs. M. Zamir, T.W.R. Macfarlane and I.C. MacDonald. Dr. MacDonald obtained the old porcine renals for me from the local abattoir.

Mr. R. Kratky, Mr. C.M. He and Mr. M. Carson: My accomplices; for their guidance, help and support. Although I often wondered if they really appreciated my humor, I will never forget the contributions they have made to my 'education'.

Mr. J. Ivey and Mr. D. Kim: Summer students who helped me construct optically clear flow models of the human infrarenal aorta and serially sectioned human aorto-iliac bifurcations, respectively.

Dr. R. Rankin and film clerks, Department of Radiology, University Hospital: for their help in obtaining and reading aortograms and computed tomographic images of normal infrarenal aortas and images of infrarenal aortic aneurysms.

Pathology Departments at University Hospital and Victoria Hospital, and Dr. Ross Armstrong at Victoria Hospital for specimens

Dr. M. Nakamura: for allowing me to present the preliminary results of the finite element analysis of flow through an expansion zone.

Mr. and Mrs. J.W. McCutcheon: for establishing the Terence W. Gilmore Memorial Scholarship. Their financial contribution enabled me to pursue my research interests and enabled me to share my discoveries with Mrs. Jean Gilmore and family. The scholarship provided me with the unique opportunity to attend several conferences within Canada, the United States as well as the United Kingdom.

My family: Marlene, Kim and Frank. The support, enthusiasm and encouragement that they have provided me during both the undergraduate and graduate programs were appreciated greatly and will not be forgotten.

Table of Contents

List of Tables

List of figures

Chapter 1

Introduction

1.1 Objectives

Localized arterial diseases such as atherosclerosis and aneurysms may be due to hemodynamic disturbances such as fluid shear stress at the arterial wall. In spite of the fact that arterial geometry plays a crucial role in altering velocity profiles, there is little detailed information about the geometry of arteries, particularly near bifurcations where these diseases are more prevalent. Arterial bifurcations can be grouped based on their location. The bifurcations associated with the human cerebral circulation and the porcine kidney are muscular arterial bifurcations (I will refer to these bifurcations as muscular bifurcations) while the branches of the human aorta are elastic arterial bifurcations (called elastic bifurcations). The cerebral bifurcations, studied previously by Macfarlane (1985) tend to develop aneurysms at the apex of the branch while aneurysms in the human aorta tend to develop in the region between the aorto-renal and aorto-iliac junctions, the so-called straight section of the abdominal aorta. Renal arterial bifurcations do not develop aneurysms at the flow divider. If arterial geometry is an important factor in the development of aneurysms, then the geometry of the human cerebral and iliac bifurcation must be different from the geometry of the renal bifurcation. If there is no geometrical difference between these bifurcations, then arterial geometry is not the major factor responsible for aneurysm development. This assumes that all aneurysms are the same, and this may not be true, particularily since brain aneurysms are saccular and at the apex of bifurcations while abdominal aortic aneurysms are fusiform and develop in the straight sections of the aorta.

When these studies were started in 1989, there was a great debate in the literature over which clinical imaging modality (i.e. ultrasound, computed tomogra-

phy (CT), aortography or magnetic resonance) provided the most accurate representation of human arterial geometry in both normal patients and in patients with arterial disease (Amparo et al., 1985; Bandyk, 1989; Tabbara et al., 1991). This debate continues today. Although rapid advances have been made recently in both imaging speed and resolution, the lack of detailed information describing *in vitro* and *in vivo* arterial bifurcation geometry make it impossible to calculate the accuracy of these modalities. In the following chapters, I will compare arterial bifurcation geometry measured from both muscular (porcine renal bifurcation and human cerebral bifurcations) and elastic bifurcations (human aorto-iliac bifurcations). All of these bifurcations are planar Y-junctions. Arterial bifurcation geometry was studied:

(1) ***in vitro:*** from 10 to 40μm serial sections of pressure-fixed specimens of 13 porcine renal and 14 human aorto-iliac bifurcations (Chapters 2, 3 and, 4), and,

(2) ***in vivo:*** from 17 aortograms and 25 CTs of the human infrarenal aorta (Chapter 5).

1.2 The role of arterial bifurcation geometry in arterial disease

In this thesis, I have defined an arterial bifurcation as the division of one vessel into two daughter vessels. Arterial bifurcations have been the focus of intense scrutiny since these regions are predisposed to the development of atherosclerotic lesions. Atherosclerosis is a patchy arterial disease that occurs near bends and branches and is characterized by intimal lipid accumulation, elastin fragmentation and reduplication, and smooth muscle proliferation. Lipid accumulation continues with time resulting in wall thickening and narrowing of the luminal space available for blood flow. Partial or complete arterial occlusions can have catastrophic

consequences depending on the location and the severity of the constriction since reduced blood flow through the coronary arteries and the cerebral arteries result in heart attacks and strokes, respectively. Combined, heart attacks and strokes remain the leading cause of death in North America.

The localization of atherosclerotic lesions near bifurcations has led several investigators to suggest that bifurcation geometry may play an important role in the localization of atherosclerosis (Friedman et al., 1983; Bargeron et al.,1986; Ku et al., 1989). The patchy distribution of atherosclerotic lesions near bends and bifurcations is thought to be due to either high shear stress (Fry, 1968) or low shear stress (Caro et al., 1971). Shear stress is a frictional force that acts parallel to the luminal surface of arteries and in the direction of blood flow. The magnitude of the resulting shear stress is proportional to both blood viscosity and the velocity gradient across the radius of the artery. Changes in arterial diameter can alter significantly both blood flow velocity and the magnitude of the shear stress that acts on the artery wall. Current instrumentation is unable to measure blood flow velocity and shear stress at the wall. Many authors have studied flow patterns in Y-bifurcations using rigid, transparent models of arterial bifurcations (Brech and Bellhouse, 1973; Caruso and Ferreri, 1975; Feurstein et al., 1976; Malcolm and Roach, 1979; Walburn and Stein, 1980) and have reported complicated flow patterns distal to the apex of a Y-bifurcation. Mathematical simulations of bifurcation flow patterns have been reported that were based on non-physiological bifurcation geometry (Lynn et al., 1972; Kandarpa and Davids, 1976; Yung et al., 1990; Thiriet et al., 1992). In all cases, the models were designed with long, straight parent and daughter branches that were fused at a predetermined angle forming a symmetrical Y-bifurcation. Comparisons among these models are difficult to make due to the large variations in tube diameters, branch angles and flow parameters used by different authors.

Friedman and Ehrlich (1984) examined the effect of curvature in the human iliac artery on wall shear stress both numerically and experimentally. A two-dimensional (2D) numerical model and a rigid, hollow, three-dimensional model of the bifurcation were constructed based on the geometry measured radiograpically, *in vitro*. The results of this study showed that by incorporating *in vitro* arterial geometry in numerical models, both flow velocity and shear stress can be modelled accurately.

The efficiency of branches to divert flow into two branches has been examined using optimality principles by measuring branch angle and branch diameter (Zamir, 1976). Zamir et al. (1985) examined branch diameters and three-dimensional (3D) branching angles from casts of the entire rat cardiovascular network made at physiological pressure. The results of this study were similar to predicted results of Murray (1926a,b). Zamir concluded that: (1) branch diameters are a compromise between lumen volume and minimum pumping power, (2) branch angles minimize both volume and power as well as minimizing drag forces exerted by blood on endothelial cells, and (3) in 253 of 309 samples, the angle between the parent branch and the plane containing the daughter branches was <5° while branch angles in the remaining locations were <10°. Although my experiments will not address the optimality of bifurcation design, Zamir's data showing that bifurcations are planar suggest that errors due to my assumption that the bifurcations are planar, are negligible.

The mechanical properties of arteries are also affected by changes in arterial diameter since circumferential tensile stress, σ, is defined as:

$$\sigma = Pr/t, \qquad (1)$$

where, P= mean arterial pressure (in Pa),

r= luminal radius (in mm),

and t= cross-sectional wall thickness (in mm).

Laplace's law (1) can be applied to thin-walled, isotropic materials. Since systemic

arteries are neither thin-walled nor isotropic, this relationship is probably not a valid method to calculate circumferential tensile stress. Burton (1962) calculated the circumferential wall tension of a thick-walled artery by incorporating the inner and outer radius in the calculation. As a result, circumferential wall tension, T, is described by

$$T = P_i r'_i - P_e r'_e \qquad (2)$$

where P_i and r'_i are internal pressure and radius, respectively, and P_e and r'_e are external pressure and radius, respectively. If we incorporate inner and outer radii into (1), we obtain the following expression for circumferential tensile stress:

$$\sigma = (P_i r'_i - P_e r'_e) / t \qquad (3)$$

Although I have not attempted to study the elastic properties of arterial bifurcations, it is obvious that information describing both luminal arterial radius and arterial wall thickness variation is highly relevant for these types of calculations.

1.3 The rationale behind the branch locations studied

Macfarlane (1985) studied pressure-fixed, human cerebral arterial bifurcations and showed the presence of large, linear changes in luminal cross-sectional area both proximal and distal to the apex. Human cerebral arteries are thin-walled, muscular Y-bifurcations composed of smooth muscle cells and a single, intimal layer of elastin and are prone to both atherosclerosis and aneurysms. This is unlike most of the elastic branches along the aorta that arise as T-junctions with the exception of the aorto-iliac.

Since Macfarlane limited his study to the cerebral circulation, it was unclear whether aneurysm formation in cerebral bifurcations was due to the single layer of

elastin or due to large changes in luminal cross-sectional area. To answer this question, I wanted to compare Macfarlane's results with the geometry of the primary bifurcation of the human renal bifurcation since this is also a muscular Y-bifurcation, although it has both internal and external elastic laminae. Since autopsy samples were extremely difficult to obtain due to the large demand for kidneys by transplant patients, I chose to examine the porcine renal bifurcation. The primary renal bifurcation is a muscular Y-bifurcation but was also planar which simplified greatly the geometrical analysis. Previous studies have shown that porcine tissue is a good model of human arteries since they are similar histologically as well as in calibre (Pond and Houpt, 1978). The results of this study are presented in Chapter 2.

The area taper in the porcine renal and human cerebral bifurcations were not significantly different ($p>0.05$). This suggested that branch geometry does not predispose the flow divider of the cerebral bifurcations to aneurysms; however, the composition of the bifurcation could play an important role in aneurysm development. The cerebral arteries are unique due to their single layer of elastin, while renal bifurcations and other muscular bifurcations have both an internal and external elastic layer. Since both cerebral aneurysms (Stehbens, 1975) and abdominal aortic aneurysms (He, 1992) contain no elastin, geometrical differences associated with the composition of arteries must be considered. In Chapter 3, I have presented in vitro changes in both geometry and wall thickness in the human aorto-iliac bifurcation. The aorto-iliac is an elastic Y-bifurcation that branches from the distal end of the abdominal aorta to two elastic common iliacs.

1.4 The effect of patient age on arterial geometry

The elastic properties of normal arteries allow the vessel to dilate during systole and accommodate large blood volumes (approximately 80 ml/beat), and to recoil during diastole and provide an extra push to blood entering the periphery. With age,

arteries become less distensible due to changes in wall thickness. Increases in arterial wall thickness result from the development of atherosclerotic plaques and/ or hypertension. Further changes in elastic properties can be attributed to elastin fragmentation, an increase in total wall collagen with age (Robert et al., 1987) and/ or an increase in the number of collagen cross-links.

Although the severity of atherosclerosis increases with patient age, previous studies have ignored changes in bifurcation geometry with patient age. Changes in cross-sectional area with age have important implications for flow patterns as well as for the shape of the bifurcation. In order to examine the effect of patient/animal age on bifurcation geometry, porcine renal arteries were examined from two groups: young pigs (n=7, age 6-14 weeks) and old pigs (n=6, age >52 weeks). Both arterial geometry and changes in parent cross-sectional wall thickness were examined from human aorto-iliacs that were harvested at autopsy from a wide age range (1 day to 76 years).

1.5 *In vivo* arterial geometry

The experiments presented in Chapters 2 and 3 were performed on isolated, pressure-fixed arteries that were embedded and sectioned. *In vitro* studies are advantageous compared to *in vivo* ones since arteries can be stained, cleaned of excessive tissue, and positioned precisely so that the best image of the sample is obtained. The major limitation of in vitro studies is that the artery is no longer subjected to physiological conditions that are present in the body. These conditions include: tethering of arteries to their surroundings, pulsatile blood pressure and smooth muscle tone.

In vivo geometry of the human infrarenal aorta (region between renal arteries and the aorto-iliac bifurcation) was examined using both aortography and computed tomography (CT). I wanted to examine the geometry of either the human aorto-iliac

bifurcation or the primary bifurcation of the human renal artery. This would have enabled me to compare directly the geometry of these bifurcations measured both in vitro and *in vivo*. It remains extremely difficult to examine *in vivo* arterial bifurcations with current imaging modalities due to the complex changes that occur in arterial geometry over relatively short distances and the fact that CT 'cuts' are averaged over 5mm thick sections.

Infrarenal aortic geometry was examined in two patient groups: normals (n=8, mean age = 64 ± 3 yrs, S.E.M.) and patients with infrarenal aortic aneurysms (n=9, mean age= 69 ± 3 yrs). The geometrical analysis was performed using both aortograms and CT images of the aorta since no one imaging modality provided an accurate 3D image of the infrarenal aorta.

Images from the aortograms of the infrarenal aorta from both patient groups included the aorto-iliac bifurcation; CT cross-sections in the bifurcation were difficult to analyse. *In vivo* infrarenal aortic diameter variation was measured from antero-posterior projection aortograms.

In summary, the objectives of the studies presented in the following chapters are:

(1) to examine *in vitro* bifurcation geometry of:
   - a muscular Y-bifurcation (porcine renal) and compare it to an elastic Y-bifurcation (human aorto-iliac),
   - compare arteries of both types at different ages, and,

(2) use *in vivo* techniques to study infrarenal aortic geometry in both normal patients and patients with infrarenal aortic aneurysms.

Chapter 2

Geometrical analysis of the porcine renal bifurcation[1]

2.1 Introduction

Human cerebral arteries are thin walled, muscular arteries that deliver blood nutrients to the brain. These arteries are predisposed to the development of both atherosclerosis and aneurysms. Cerebral aneurysms occur almost exclusively at the apex of cerebral arterial bifurcations (Hassler, 1961). It remains unclear why aneurysms form primarily at the apex of cerebral bifurcations and not at the apex of other muscular arteries.

Macfarlane (1985) reported large, linear luminal area changes both proximal and distal to the apex of human cerebral bifurcations. The luminal cross sectional area of the parent branch increased linearly by 94.5% (±5.0% S.E.M.) up to the apex and decreased linearly by 36.9% (±4.0% S.E.M.) distal to the apex. The apex corresponded to the location of maximum cross-sectional area. These large changes in luminal must have significant effects on both blood flow velocity and wall shear stress. Although fluid mechanical factors such as shear stress, have been implicated in the localization of atherosclerotic lesions, the role of bifurcation geometry in aneurysm development is uncertain.

Since Macfarlane's studies (1985) were limited to the cerebral arteries, it was

---

[1]This study has been published ; MacLean, N.F., Kratky, R.G., Macfarlane, T.W.R., and Roach, M.R. (1992). Taper: an important feature of Y-bifurcations in porcine renal arteries and human cerebral arteries. J Biomechanics 25: 1047-1052. Some of the text and figures were reproduced with the permission of Pergamon Press. I was responsible for sample preparation, sectioning, data analysis and preparing the manuscript. Mr. Kratky helped me to develop the staining technique while Dr. Macfarlane allowed me to use his computer and software. The initial measurements on 4 adult pig arteries were done as part of a Biophysics 480 project, but all the rest were done as part of the Ph.D. project.

unclear whether the large luminal area changes reported near the apex were unique to the cerebral circulation, or whether these large luminal area changes were present in other muscular arteries. To answer this question, I examined luminal area changes in the primary bifurcation of the renal artery. The primary bifurcation of the renal artery is a muscular Y-bifurcation that delivers blood to one of two kidneys.

The results of this study might help to explain whether luminal geometry is important in the localization of aneurysms at the apex of cerebral bifurcations but not other muscular Y-bifurcations. These results could also have implications on the way in which future hemodynamic studies of Y-bifurcations are interpreted.

2.2 Methods

2.2.1 Tissue selection

Porcine renal arterial bifurcations were chosen as representative of muscular systemic bifurcations. Although the renal artery is elastic at the aorta, the vessel becomes muscular before the first bifurcation, the region studied here. The renal bifurcation has planar geometry (i.e. parent trunk and daughter branches lie in the same plane) which simplified the analysis. To separate the effects muscular composition and patient/animal age, porcine renal arteries were harvested from two groups of animals; the first group of arteries was collected from mature animals at the abattoir (age >52 weeks, n=5) and the second group was obtained from donor, juvenile mini-pigs used for bowel transplants at University Hospital (age 6-14 weeks, n=7). Since there was a large difference in animal age as well a difference in animal strain, we decided to separate the tissue into two groups based on age. Changes in cross-sectional luminal area were assessed in the renal arterial bifurcation from the block face as serial sections were removed (Macfarlane, 1983b). Distortions due to tearing and processing encountered commonly in histological sections were removed completely with this method.

2.2.2 Formalin fixation and sectioning

Porcine renal arterial bifurcations were harvested from the animal with the abdominal aorta and kidney still attached and excess connective tissue was removed. The kidney was left attached to preserve the angle of the bifurcation. Rigid plastic tubing connected the proximal end of the aorta to a pressure-fixation apparatus. The bifurcation was made pressure tight by tying-off the distal end of the aorta, the renal vein and the ureter. *In vivo* arterial geometry was obtained by pressure-fixing the vessel with 10% buffered formalin at mean porcine arterial pressure of 140 mmHg (Pond and Houpt, 1978) for a period of three hours. The effect of smooth muscle tone in these vessels was reduced by leaving the samples in saline at 4°C for one day prior to pressure fixing the vessels. Kratky et al. (1991) found that recoil in pressure fixed canine carotid arteries reached a minimum of 5% in diameter and 10% in length following three hours with this fixative. The precise location of the luminal surface of the artery was enhanced in two ways: (i) white latex paint was used as the embedding compound, and (ii) the sample was stained with methylene blue (100mg / 100ml) for one hour and excess dye removed with saline. A Kryomat unit (Leitz) was used to freeze the latex paint on the stage of the sledge microtome by circulating refrigerated methanol (T= -35°C) through both the stage and the knife of the microtome. The parent trunk of the bifurcation was embedded perpendicular to the microtome stage to ensure cross-sections were produced. Samples were mounted vertically so that the daughter branches were closest to the blade. Initially, the lumen of the stained artery was filled with latex paint prior to building-up the embedding block around the exterior of the vessel. The block was allowed to freeze for one hour prior to sectioning to achieve thermal equilibrium within the block. Macfarlane (1985) showed volume changes of the latex block due to freezing were negligible (±0.03%).

The length of samples sectioned was limited by the vertical distance between the blade and the stage which was 2.5 cm. Serial sections were cut at 20.00±0.01μm increments from the block face by sliding the embedded artery and stage under a refrigerated knife (T= -35°C). During the sectioning process, the top surface of the block was recorded with an inverted video camera (Sony, AVC 3260) and a 55mm Nikkor close-up lens which was mounted at a constant height (Figure 2.1). The video signal from the camera was interlaced with a time/date generator and stored on a video cassette. The video tape was replayed through an IBM-compatible computer equipped with a frame-grab board. Due to the large number of sections produced by this process (800-1200), I chose to examine every tenth slice. The luminal area was measured digitally using existing software (ImagePro II) which required the operator to outline the lumen with a mouse (Logitech). Approximately fifty points were used to trace the luminal surface of the artery. Each of the two lumens produced in slices through the daughter region were analysed separately. Since the digitized image was traced from a monitor composed of pixels which are not square it was necessary to calibrate the area measurements by video recording a scale bar which was mounted at blade level and then rotated by 90° and recorded a second time. Calibration with the scale bar allowed me to convert area measurements in $(pixels)^2$ to units of $(mm)^2$.

The methods used in this study differ slightly from Macfarlane's (1985) since human brain arteries were pressure fixed at 100 mmHg for 24 hours while attached to the brain (3hrs for renals at 140 mmHg), cerebrals were embedded with black latex paint in the lumen and white paint around the outside, and sections were collected at 10μm increments (20μm increments from renals).

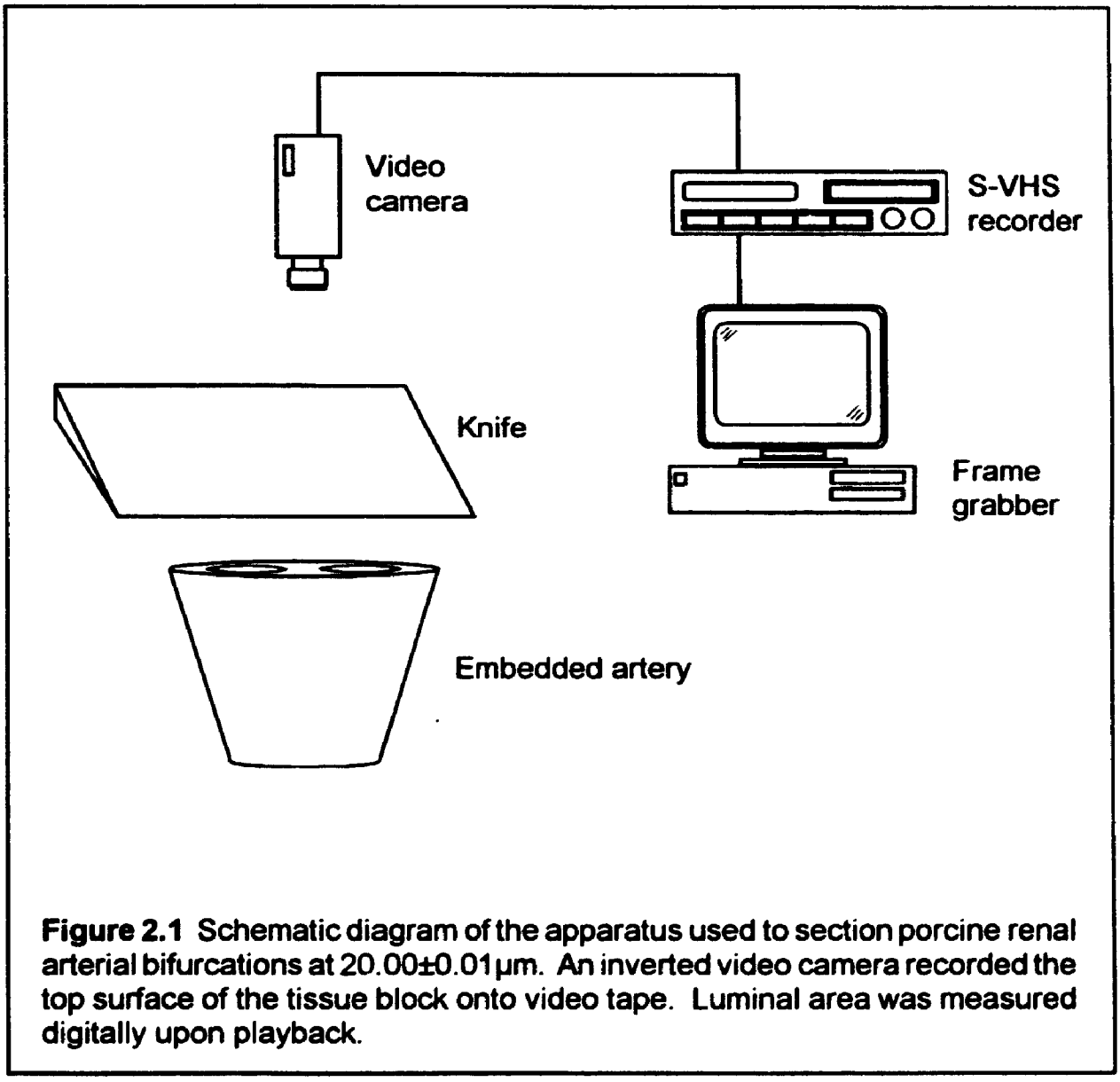

Figure 2.1 Schematic diagram of the apparatus used to section porcine renal arterial bifurcations at 20.00±0.01μm. An inverted video camera recorded the top surface of the tissue block onto video tape. Luminal area was measured digitally upon playback.

2.2.3 Data analysis

Careful mounting of the planar bifurcations prevented oblique sectioning of the parent trunk; however, sections of the daughter branches distal from the flow divider were cut obliquely. The oblique cross-sectional area is related to the transverse area or 'true' cross-sectional area through the cosine of the half-branch angle, defined as the angle subtended by the axis of symmetry of the parent trunk and one of the daughter branches. The maximum error introduced by not correcting oblique sections in bifurcations which possessed half-angles less than 25° was <9%. This error was insignificant when compared to the large changes present in luminal cross-sectional area. Any method of correcting cross-sectional area caused a discontinuity in the area-location curve. In addition, curvature in the branches made determination of branch angle difficult. As a result, we elected not to correct our data for branch angle and excluded samples with half-angles greater than 25°. Only four samples were rejected prior to the study for this reason.

2.2.4 Geometrical parameters

(i) **Area ratio:** The area ratio was defined as the ratio of the summed luminal area of the daughter branches to that of the parent branch measured one parent-tube diameter in both directions from the apex. The parent tube diameter was calculated assuming that the lumen was circular in cross-section.

(ii) **Area taper:** Slope of Area-length curves: Luminal area measurements obtained from digitized serial sections of porcine renal arterial bifurcations were plotted as a function of distance from the flow divider (in mm). The cross-sectional area was largest at the flow-divider. The luminal area measurements were divided by the value at the flow divider to normalize the data. Normalization was necessary to compare samples of different diameters. Sections of the parent trunk were assigned negative distances from the flow divider while daughter sections were

positive distances. The values reported for luminal area of daughter branches were for the sum of the two branches. Taper was defined as the slope of the area-location curve for both parent and daughter branches, and was calculated as the change in area (in mm^2) from the apex to its minimum value divided by the distance (in mm) over which the change occurred. It is noted that the definition of taper is different from the dictionary and from other researchers' definition of taper since I have defined it based on area while taper is usually based on a change in diameter. Since mean blood flow velocity equals flow/unit area, area taper is more useful than diameter taper for determining if the flow is accelerating or decelerating. If the lumen is circular in cross-section, then extrapolations can be made between area taper and diameter taper. However, as the bifurcation is approached, the lateral diameter must increase to form the branches. If antero-posterior diameter decreases to maintain constant area, then area taper might be zero while the taper of the diameter would be negative (flaring) in the lateral direction, but positive (taper) in the antero-posterior direction. This shape change will alter the velocity profile. Thus area taper and diameter taper have quite different implications. Taper in the parent branches of both renal and cerebrals was negative and corresponded to an expansion in cross sectional area in the direction of flow while there was a narrowing (i.e. taper) in the daughter branches.

Macfarlane (1985) presented his data as individual area values. I have used his data to calculate tapers in order to compare the geometry of cerebral and renal bifurcations.

2.2.5 Statistical analysis

Changes in luminal cross-sectional area of porcine renal arterial bifurcations of two age groups (age 6-14 wks, n=7; >52 wks, n=6) were compared to each other as well as to changes measured in human cerebral arterial bifurcations (Macfarlane,

1985) based on the taper from parent and daughter vessels, separately, using an Analysis of Variance (ANOVA, $p<0.05$). The significance of the taper was determined from the correlation coefficient (r^2) and p-value using a p-value cut-off of 0.05 (McClave and Dietrich, 1986). The mean area ratios obtained from seven young and six old porcine vessels were compared using a two-tailed t-test ($p<0.05$).

2.3 Results

2.3.1 Cross-sectional luminal area

The area of the porcine renal arteries, like those of the human cerebrals, was greatest at the level of the flow divider. Cross-sectional luminal areas proximal to the flow divider increased in the direction of the apex while those distal to the flow divider decreased (Figure 2.2a,b). The percent change in luminal cross-sectional area in the parent branch (dA_p) as well as the summed luminal area change in the daughter branches (dA_d) was calculated using the maximum area at the apex and the same length of both parent and daughter vessels. The length of the renal artery to the first bifurcation as well as the length of the daughters to the second bifurcation were variable due to biological differences; as a result, the lengths over which the total area changes were measured was variable. Luminal cross-sectional area increased in the parent branch by 47.0% (±7.6% S.E.M.) in the old pig renal and by 35.5% (±7.6% S.E.M.) in the young vessels (Tables 2.1 and 2.2). Macfarlane (1985) showed that the luminal area of the human cerebral arteries increased by 94.5% (±5.0% S.E.M.) proximal to the flow divider (Table 2.3).

2.3.2 Area taper

The variable, area taper, was developed to avoid differences in total area change that were due to differences in the vessel segment lengths, between animals. Area taper was calculated as the change in luminal cross-sectional area

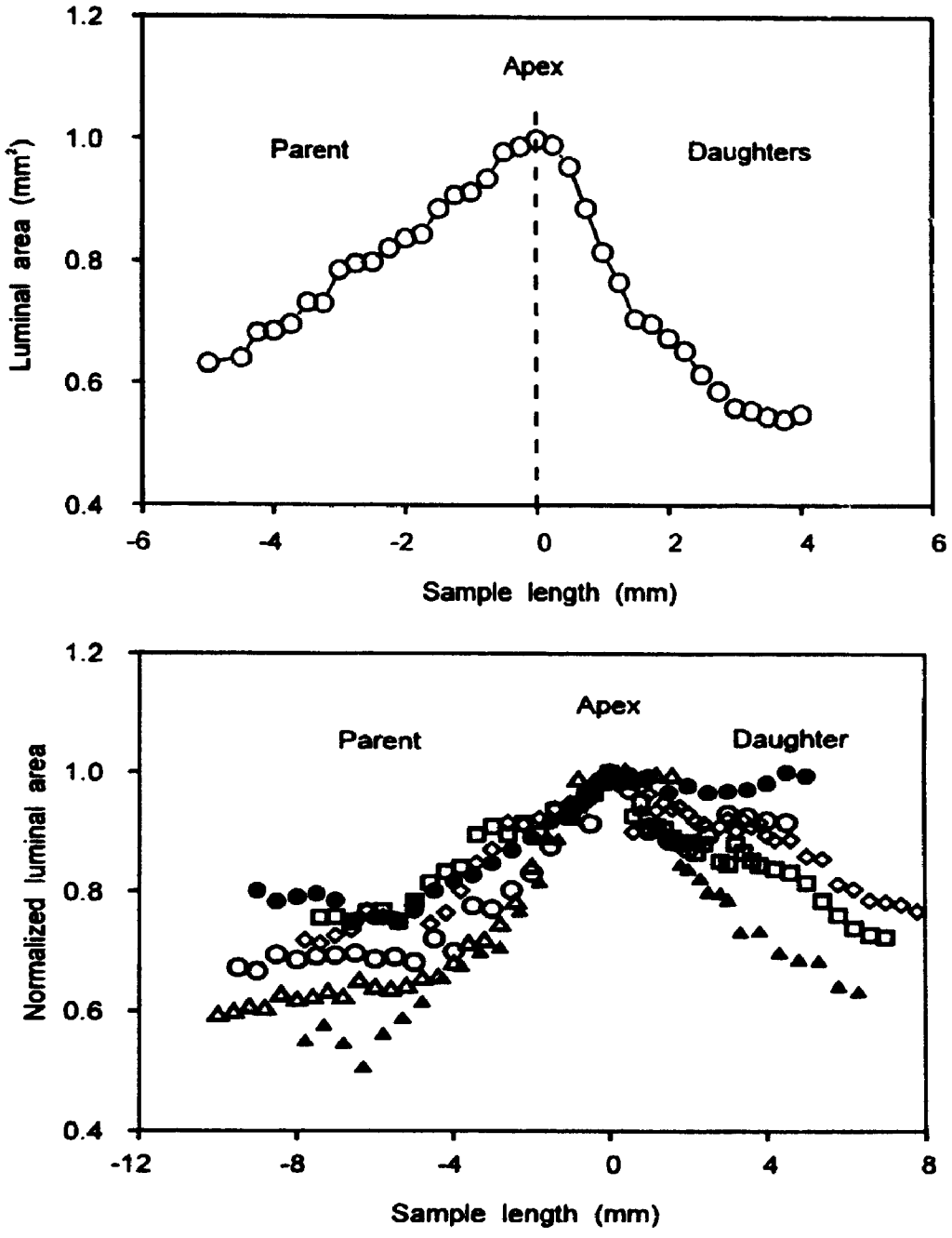

Figure 2.2 Old porcine renal bifurcations. (a) Large changes in luminal cross-sectional area were observed in the parent trunk from old porcine renal bifurcations as well as in the daughter regions (data from OP-5 shown here). Area in the daughter region represents the sum of both daughters. (b) Luminal area was normalized with respect to the area at the apex in each of the seven bifurcations shown (i.e. each symbol represents one old porcine renal bifurcation). This figure was reproduced from Journal of Biomechanics with permission from Pergamon Press.

Table 2.1 Luminal area and taper from old pig group (>1year)

Sample	Parent diameter (mm)	Area change %		Area ratio	Area taper (mm)	
		Parent	Daughter		Parent	Daughter
OP-1	5.0	45.5	12.7	1.1	-1.8	1.6
OP-2	5.6	32.9	3.1	--	-1.3	--
OP-3	5.4	68.9	0.7	--	-2.5	--
OP-4	3.6	83.6	31.6	1.2	-2.2	1.6
OP-5	3.4	37.1	19.5	1.1	-2.1	1.4
OP-6	7.7	13.9	27.9	--	-1.1	4.0
Average (±S.E.M.)	5.1 (0.7)	47.0 (10.5)	15.9 (5.2)	1.2 (0.1)	-1.8 (0.2)	2.2 (0.5)

Parent diameters were calculated from the minimum cross-sectional area in the parent branch. Area change represents the percentage change of luminal area in either parent or daughter branches relative to the area at the apex. Area ratios were defined as the ratio of summed luminal area of the daughter branches to that of the parent branch measured one parent tube diameter from the apex. Taper is defined as the change in luminal area divided by the distance from the apex over which this change occurred.

Table 2.2 Luminal area and taper from young pig group (6-14 weeks).

Sample	Parent diameter (mm)	Area change %		Area ratio	Area taper (mm)	
		Parent	Daughter		Parent	Daughter
SP-1	3.9	48.8	14.3	1.5	-1.6	1.2
SP-2	4.2	66.3	17.6	1.1	-1.3	2.1
SP-3	2.2	47.8	60.4	0.9	-1.7	1.1
SP-4	2.1	33.3	62.8	0.6	-0.7	1.0
SP-5	1.7	10.1	79.9	0.3	-0.3	1.5
SP-6	3.2	27.9	40.8	0.4	-0.7	2.3
SP-7	2.7	14.5	26.4	0.9	-0.7	1.4
Average (±S.E.M.)	2.8 (0.3)	35.5 (7.6)	43.2 (9.5)	0.8 (0.2)	-1.0 (0.2)	1.5 (0.2)

Table 2.3 Luminal area changes (%) were obtained from Macfarlane (1985, p.p. 62-94). I calculated both area ratio and taper from his data.

			Area change %			Area taper (mm)	
Location	Age/Sex	Parent diameter (mm)	Parent	Daughter	Area ratio	Parent	Daughter
3-Rt. Mid.	65 M	1.6	87.4	31.7	–	-0.7	1.3
4-Rt. Mid.	65 M	0.8	111.9	42.8	–	-0.8	1.1
1-Lt. Ant.	68 F	1.8	97.6	28.6	–	-1.9	1.5
3-Lt. Ant.	65 M	1.4	102.7	50.7	0.8	-1.0	1.4
2-Rt. Ant.	40 M	1.6	76.9	42.1	–	-2.0	1.4
1-Rt. Ant.	68 F	1.7	90.5	25.4	–	-2.3	2.0
Average	61.8	1.5	94.5	36.9		-1.5	1.5
(±S.E.M.)	(4.4)	(0.2)	(5.0)	(4.0)		(0.3)	(0.5)

Table 2.4 Summary of mean data (±S.E.M.) from young and old porcine renals and human cerebral bifurcations.

	Young pig	Old pig	Pooled porcine data	Human cerebral
Area Change (%)				
Parent	35.5±7.6	45.7±10.5	40.1±9.1	94.5±5.0
Daughter	43.2±9.5	15.9±5.2	29.5±7.4	36.9±4.0
Taper (mm)				
Parent	-1.0±0.2	-1.8±0.2	-1.39±0.2	-1.5±0.2
Daughter	1.5±0.2	2.2±0.5	1.73±0.2	1.5±0.2
Area Ratio	0.8±0.2	1.2±0.1	0.91±0.1	--

Young and old porcine renals were compared with human cerebral data using an ANOVA with a cut-off of $P<0.05$. No significant difference was found between area-taper in young and old porcine renal and human cerebral arteries in the parent and daughter branches, respectively.

per unit length of artery and has units of mm^2/mm or mm. A positive value implies flow is accelerating while a negative value implies it is decelerating. This parameter is valid only if it is constant along the length of the sections. For example, it is not valid to use only the first and last values unless the change in luminal area is linear. This will become important in Chapter 5 when aortic aneurysms are analysed. The number of sections analysed must be sufficient to ensure that local area changes are detected. All area tapers were significantly different from zero for both parent and daughter branches of both young and old porcine renals as well as from human cerebral bifurcations ($p<0.05$). These Y-bifurcations showed the same trend: negative taper (flaring) proximal to the flow divider followed by positive taper distal to the flow divider with the transition at the flow divider where the area was the greatest (Table 2.4). Statistically, there was no significant difference between the mean area tapers measured in the parent branches of both young and old porcine renal arterial bifurcations and human cerebral arterial bifurcations (ANOVA, $p>0.05$, $F_{2,16,0.05} = 3.24$). It was noted that there are two possible reasons why no difference was found between these groups: (1) that there was actually no significant difference between these samples, or (2) that any difference between these groups was small, and larger sample sizes would have been required in order to detect a difference. Area taper present in the summed daughter branches failed to pass the normality test ($p= 0.013$) required to proceed with an ANOVA. As a result, a non-parametric analysis was performed using Sigmastat (v1.01, Jandel Scientific) on the daughter branch taper. A Kruskal-Wallis one-way ANOVA (based on median values) was used as well as a Chi-squared approximation for P ($p= 0.304$). There was no significant difference between the area tapers in the daughter branches ($p>0.05$).

2.3.3 Area ratio

The mean area ratios (± S.E.M.), calculated one parent-tube diameter proximal and distal to the flow divider of the old pig group (1.2 ± 0.1) were not significantly different ($p>0.05$) from the mean area ratio of the young pig group (0.8 ± 0.2). Since the absolute areas of both change, but area ratio was approximately unity, there should be large changes in mean flow velocity through this region. However, since taper was present in both regions, mean velocity will decrease in the parent, but increase in the daughters as a function of distance from the apex. Thus I propose that area taper is a more reliable means of predicting mean velocity changes near bifurcations than is the usual parameter of area ratio.

2.4 Discussion

The goal of this study was to determine if systemic Y-bifurcations and cerebral Y-bifurcations had similar changes in geometry. Since our measurements showed large changes in luminal area occurred over relatively short distances, we concluded that the measurement of area ratio described by others could be subject to large variations if the location of the measurement was not precise (because of the assumption that the vessels were cylindrical). For this reason, I concluded that tapers were probably more important than area ratios.

I concluded, based on the magnitude and the variance of the taper in the parent and daughter branches, that young and old porcine renal arterial bifurcations were not different. Although there is a chance that these tapers were significantly different (i.e. representing a Type II error; retaining a false null hypothesis) the ANOVA showed that the variation within samples ($SS_{within} = 5.6$) was larger than the variation between groups ($SS_{between} = 2.3$). In order to predict the sample size required to demonstrate a significant difference, we must assume that new samples would be drawn from a population having the same distribution as the samples studied

previously. From F-tables (Witte, 1989), the calculated F-value of 3.24 would become critical with 40 degrees of freedom ($F_{2,40,0.05} = 3.23$). The number of samples required can be calculated from:

$$N_{samples} = df_{within} + N_{groups} \quad (4)$$

With three groups, forty-three samples would be required to demonstrate a significant difference between the magnitudes of the area-tapers reported in Table 3.4. As a result, it would be necessary to study twenty-four more bifurcations to show that a difference exists (assuming that these new samples could be drawn from the same population as the samples studied previously).

Ludin et al. (1971) examined the alteration in renal artery diameter from abdominal aortograms of children (n=127), adults (n=458) and autopsy specimens (n=27) which included both normal patients and those suffering from renal disease. Ludin et al. defined a tapering parameter to be the relative difference between diameters measured at 1 and 3cm from the origin. Both renal artery diameter (at origin) and tapering parameter were statistically independent of age, sex and blood pressure at time of admission. Although Ludin's group showed that negative taper was present in the parent branch of the renal artery, our study showed that area changes were linear and were also present in the daughter branches. Ludin calculated diameter taper while I used area taper. As noted in Section 2.3.2, diameter taper can be misleading if the shape of the lumen changes.

If I compared the ratios of the mean area taper in the daughter branches to the mean taper in the parent trunk for both young and old samples, the young bifurcations would have a ratio of -2.22 (±0.68 S.E.M., n=7) and the old pigs would have a value of -1.54 (±0.76 S.E.M., n=4). The taper ratios were compared using a Student's t-test and were not significantly different ($p>0.05$). The ratio of the tapers provides a measure of the asymmetry present between the area changes present in the parent and the daughter branches of one sample. The effect of the asymmetry

in the ratio of daughter to parent taper on bifurcation flow patterns remains unknown.

Luminal cross-sectional area changes in the porcine renal and human cerebral bifurcations (Macfarlane, 1985) were not significantly different ($p>0.05$). Since both bifurcations are classified as muscular Y-bifurcations, this might suggest that luminal area changes alone are probably not the cause of cerebral aneurysms. The formation of aneurysms at the apex of cerebral bifurcations might be due to the thin walled structure of the cerebral arteries and the fact that there is a single layer of elastin which is absent in aneurysms. This remains to be studied. I believe that large tapers could be present in other arteries, such as coronary and carotid arterial bifurcations. These tapers could have a significant effect on blood flow through them.

In summary, the results of this study have shown:

(1) large, linear changes in luminal area in both parent and daughter branches of porcine renal arterial bifurcations,

(2) the magnitude of the area changes did not correlate with animal age over the age range studied.

(3) the magnitudes of the area tapers in the parent and daughter branches of porcine renal and human cerebral arterial bifurcations were not significantly different based on an analysis of variance ($p>0.05$),

The implications of these results are:

(1) in the absence of separation zones, mean flow velocity must decrease in the parent trunk before reaching the flow divider. If separation zones are present, these would produce even lower shear regions which may play a role in the localization of atherosclerosis. The shape of the bifurcaiton must be considered as well.

(2) at least in the renal artery, normalized geometrical parameters seem unchanged with age while the absolute values may change as the animal grows. In this bifurcation, geometrical changes are probably not a major factor in determining why atherosclerosis develops in older animals

(3) Human cerebral bifurcations are prone to develop aneurysms at the apex of the bifurcation while renal bifurcations (either human or porcine) do not. Since there was no difference in area taper between the two groups, this is unlikely to be the parameter that explains why aneurysms develop. Before stating this conclusively, one must determine if area taper is different for cerebral arteries that have aneurysms. This study has not been done.

From the work of others, cerebral and renal arteries have localized atherosclerotic lesions near the lateral angles while the abdominal aorta has atherosclerosis diffusely along its length (from the renal arteries to the aorto-iliac bifurcation) as well as at the lateral angles. The localization of atherosclerotic lesions in these regions suggest that hemodynamic factors such as shear stress and area taper are important factors.

The aorto-iliac bifurcation is the only Y-junction arising from the aorta. All others are T-junctions which have quite different flow patterns (Karino and Goldsmith, 1985). The abdominal aorta has dramatic changes in flow in the first few days of life as the umbilical circulation which arises from the internal iliac is stopped. Similar changes early in life do not occur in the cerebral and renal bifurcations although all of the vessels grow with the animal or human.

Chapter 3

In vitro geometrical analysis of the human aorto-iliac bifurcation[1]

As pointed out at the end of Chapter 2, the aorto-iliac bifurcation is different from both cerebrals and renals as: (1) cerebrals and renals have localized atherosclerosis at the lateral angles while the aorto-iliac has diffuse atherosclerosis along its trunk as well as at the lateral angles, (2) aneurysms develop exclusively at the apex in cerebral bifurcations and proximal to the apex in the aorto-iliac and do not develop in renals, and (3) the aorto-iliac bifurcation has dramatic changes in flow within the first few days of life as umbilical blood flow is stopped. No such change in blood flow occurs in either the cerebral or renal arteries. In this chapter, I have designed a study to compare the luminal geometry of muscular Y-bifurcations to the geometry of elastic Y-bifurcations using the techniques described in the previous chapter.

3.1 Introduction

While both elastic and muscular arteries develop aneurysms, cerebral arteries develop aneurysms at the apex of bifurcations in the circle of Willis and the aorta develops aneurysms in the region between the renal arteries and the iliacs (i.e., in the relatively straight section of the abdominal aorta). Elastin is gone in both cerebral (Stehbens, 1975) and aortic aneurysms (He, 1992).

Muscular arteries have an internal elastic lamina as well as an external elastic lamina with scattered elastin throughout the media while elastic arteries have a lamellar structure with multiple layers of elastin (Wolinsky and Glagov, 1964).

The aorto-iliac bifurcation is a large calibre, elastic Y-bifurcation that delivers

---

[1]Serial sections of human aorto-iliac bifurcations were obtained with the help of Mr. D. Kim who worked with me as a summer student in 1991 and 1992.

blood from the heart to each of the legs. The elastic properties of the normal aorta allow the artery to distend during systole and accommodate approximately 80 ml of blood, and to recoil during diastole and provide an extra push to the blood entering the periphery (Avolio, 1992).

During the aging process, the human aorta becomes less distensible and so the flow and pressure waves will change. The increased stiffness also increases the speed of wave propagation along the aorta and likely plays an important role in determining peak arterial pressure since peak pressure is a function of timing and intensity of wave reflection (Avolio, 1992). Wave reflections are produced at sites of impedance changes that occur when an artery branches and produces two daughter branches in which the summed daughter luminal area is different from that of the parent. Greenwald et al. (1990) have suggested that *in vitro*, increases in wave amplification due to arterial stiffening might be offset by an increasingly negative reflection coefficient (a negative reflection coefficient will reduce pulse pressure on either side of the bifurcation).

The aorta is composed of distinct layers, or lamellae (Wolinsky and Glagov, 1964; Clark and Glagov, 1985) that consist of collagen and elastin, as well as smooth muscle cells and ground substance (glycosaminoglycans). Although the ratio of collagen to elastin varies along the aorta, the mechanical properties of the aorta also become altered by change in cross-sectional wall thickness that result from atherosclerotic lesions, hypertension, or both. Further changes in elastic properties of the aorta can be attributed to the progressive fragmentation of elastin that results from an increase in serum elastase concentration with age, as well as to a large increase in total collagen with age (Robert et al., 1987).

Changes in the arterial composition of elastin and collagen that occur with age, as well as an increase in wall thickness due to hypertension or to atherosclerosis makes it difficult to understand which factors determine both arterial diameter and

wall thickness of the aorto-iliac bifurcation. Glagov et al. (1992) have proposed that aortic luminal diameter is determined by flow forces (i.e. shear stress) while aortic wall thickness is determined by mechanical forces (i.e. tensile stress). Zarins et al. (1987) tested this hypothesis by increasing blood flow velocity in cholesterol-fed, cynomolgus monkeys via an arteriovenous fistula between the right iliac artery and vein. Six months after this procedure, there was a large increase in blood flow velocity, but there was no change in wall shear stress. During the six months, there was a large increase in the right iliac diameter and there was no significant difference between the atherosclerotic involvement of the right and left iliac arteries.

This study was designed to obtained detailed geometrical data about the human aorto-iliac region to determine if the same taper occurs there as in the muscular branches presented in Chapter 2 as well as to see if there were changes in wall thickness in the regions that are used for predicting tensile stress. Previous calculations of tensile stress have used Laplace's law which states that circumferential tension is equal to the product of pressure times luminal radius. Stress is defined as the tension per unit wall thickness. Wall thickness was assumed to be constant in previous calculations of stress. Since atherosclerosis is localized, it is important to know if there are differences in cross-sectional area and/or wall thickness in this region.

3.2 Methods

3.2.1. Tissue selection

The human aorto-iliac bifurcation was chosen for this study since the aorto-iliac is a large-calibre planar Y-bifurcation that is predisposed to arterial diseases such as atherosclerosis and aneurysms, and is available at autopsy. Autopsy samples were collected at the Children's Hospital of Western Ontario and University Hospital from fourteen patients ranging in age from 1 day to 76 years (Table 3.1). The cause

Table 3.1 Summary of patient age, sex, cause of death and fixation pressure

Autopsy number	Age (years)	Sex	Fixation pressure (mmHg)	Cause of death
V113_92	1 day	F	70	still born
V89_92	3 mo	F	70	meningitis
V100_92	9 mo	F	70	S.I.D.S.
V108_92	11 mo	F	70	S.I.D.S.
V87_92	6	F	100	trauma
V161_92	14	F	100	pneumonia
A99_92	19	F	100	leukemia
A42_92	29	M	100	cystic fibrosis
A84_92	41	F	100	connective tissure disease
A31_92	44	F	100	sepsis
A111_91	59	F	100	M.O.F.
A53_92	61	M	100	respiratory failure
A71_92	73	F	100	pulmonary embolus
A129_91	76	M	100	pneumonia

*S.I.D.S. = Sudden infant death syndrome

**M.O.F. = Multiple organ failure

of death of these patients was not directly related to the abdominal aortic disease. Variations in both luminal cross-sectional area and cross-sectional wall thickness were examined based on the method that I used to analyse the geometry of both porcine renal and human cerebral bifurcations (see Section 2.2.2.).

3.2.2. Formalin fixing, decalcifying and staining

Human aortas were collected and loose adipose tissue was dissected away. Arteries were connected to the pressure-fixation apparatus through a rigid, tight-fitting plastic tube that was inserted in the proximal end of the aorta. The aortas were made pressure-tight by tying-off the distal end of each common iliac and all of the side-branches. Each sample was fixed with 10% buffered formalin under static pressure conditions. Adult samples were fixed for three hours at 100 mmHg while juvenile samples were fixed for four hours at 70 mmHg. The difference between fixing times for young and old was to reduce the amount of recoil in the young aortas which are very distensible. Previous studies have shown that elastin retains its elasticity following aldehyde fixation (Fung and Sobin, 1981; Kratky et al., 1992). The changes in outside diameter following the release of static pressure were not examined in this study. Arteries with large amounts of elastin, such as young aortas, will be harder to fix and more recoil may occur than that reported by Kratky et al. from mature canine carotid arteries.

Calcification associated with atherosclerotic disease was present in five of the adult samples studied: A111_91, A129_91, A31_92, A53_92, and A71_92. The hardened calcium deposits were solubilized to prevent damaging the blade of microtome as well as to prevent non-uniformly thick sections. These samples were decalcified, after fixation, using a standard histological method. Each vessel was suspended vertically by threads in 12% ethylenediaminetetra-acetic acid (EDTA, pH=7.0) for one week. EDTA chelates insoluble calcium from the tissue and the

complex formed is soluble in water. This method gives superior results compared to conventional acid decalcifying agents since it avoids tissue hydrolysis (Seilly, 1982). Furthermore, Mukai et al. (1986) found that formalin fixed tissue that had been decalcified in EDTA showed the best histological preservation when compared to other decalcifying compounds: formic acid, nitric acid and Plank-Rychlo solution.

Contrast between intimal and adventitial surfaces of the artery wall and the embedding compound was enhanced by staining the vessels with 0.01% acid fuchsin solution for approximately 20 hours. Acid fuchsin provided high contrast by staining the entire vessel reddish-purple, while the embedding compound was white. The vessels were washed in isotonic saline for 24 hours to remove excess stain.

3.2.3 Tissue embedding and sectioning.

The stained vessels were mounted with the common iliac arteries toward the top and with the parent branch perpendicular to the stage of the refrigerated sledge microtome (Leitz Kryomat). Two thin-walled styrofoam containers provided both insulation and a rigid form in which the artery was embedded. The embedding compound (O.C.T., Canlab) was poured in the lumen of the vessel and then around the sample. The lower half of the sample was refrigerated by the sledge microtome at T=-30°C and required 1.5-2 hours to freeze. Liquid Nitrogen was poured over the top surface. This produced rapid freezing from the top of the block, downwards, while the refrigerated microtome froze the block from the bottom, upwards. This method enabled me to extend the length of samples that could be sectioned with the sledge microtome from a height of 2.5 to 7.5 cm. The block was allowed to freeze for one hour to reach thermal equilibrium prior to sectioning. Sections were removed

from the block face at 10μm increments in juvenile samples and at 40μm increments in adult samples. A vertically mounted black and white CCD camera (Hitachi KP M1U) recorded the top face of the block during the sectioning process while an S-VHS video recorder (Panasonic AG 7350) stored the images for future analysis.

This technique elimated most of the artifacts encountered commonly with histological sections due to tearing and folding since the lumen is measured from the digitized image of the block face rather than from individual sections.

3.2.4 Image acquisition and data analysis.

The video-taped images were digitized (Data Translation, DT2853) with an IBM-compatible computer and were analysed with software which had been developed specifically for this project. Prior to sectioning, the system was calibrated with a grid consisting of 4x4mm squares that were recorded at blade height, and then digitized. Since pixels are not square, the grid enabled me to calculate the number of pixels per mm (measured in both the vertical and horizontal directions) and to convert from units of $(pixels)^2$ to $(mm)^2$.

Once the images of the bifurcation were digitized, the luminal boundary was outlined with 35-50 points using a mouse. The luminal area was calculated based on the area enclosed between adjacent points while the location of the centroid was calculated by averaging all x- and all y-coordinates of pixels which outlined the lumen. Since the sectioning process generated between 1500 and 2400 sections per vessel, I decided to study every twentieth slice near the apex of the bifurcation and every fortieth slice away from the apex.

Following the luminal cross-sectional area calculation, the program displayed the location of the centroid and then superimposed a polar grid on the section. Wall thickness was measured in 15° increments from sections along the parent branch. The grid was oriented so that 0° was right-lateral, 90° anterior, 180° left-lateral, and

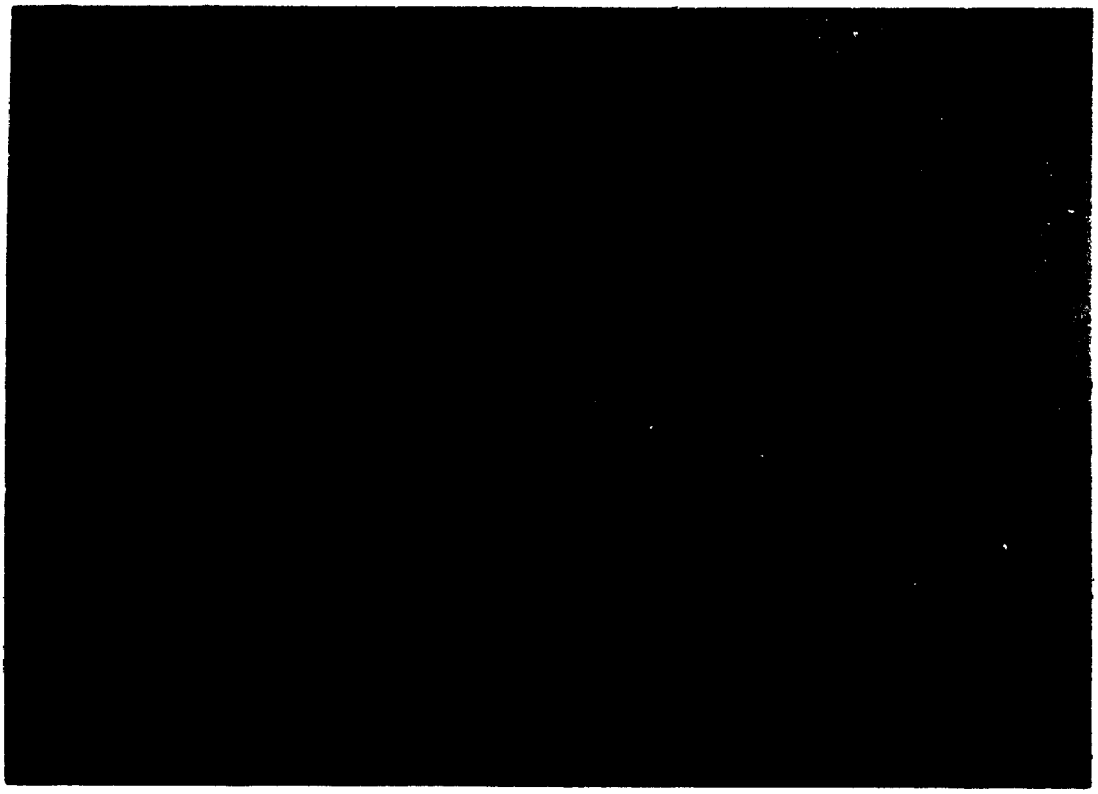

Figure 3.1 Digitized aortic cross-sectional image from a 1 day female. Luminal area was calculated by tracing the boundary of the lumen and wall thickness was measured in 15° increments using a polar grid centred on the centroid of the section (red circle). Scale bar is 1mm long.

270° posterior (Figure 3.1). The mouse was used to click on the intersection points of the intimal and adventitial surfaces of the artery with each ray. The x and y co-ordinates of the intersection points were saved as a DOS text-file which could be imported into a spreadsheet program.

The co-ordinates of the centroid of both the parent and daughter branches served two purposes:

(1) for the origin of the polar grid used to measure wall thickness variations and,

(2) to correct for oblique sections through the daughter branches.

The x and y co-ordinates of the centroids were plotted as a function of location along the vessel. Branch angles were calculated from the slope of each of these curves. The oblique cross-sectional area is related to the transverse or 'true' cross-sectional area through the cosine of the half-angle. As a result, all samples were corrected for oblique sectioning.

3.2.5 Calibration of luminal area and wall thickness measurements.

The image acquisition system and the software used to measure both luminal area and wall thickness of the human aorto-iliac was calibrated using images of washers similar to those shown in Figure 3.2. Each of the washers were recorded from a CCD video camera to S-VHS video-tape, digitized by the computer and analysed with the custom software. Luminal diameter of each image was measured in both horizontal and vertical directions using calipers. Wall thickness was measured at four locations using this technique: right-lateral, anterior, left-lateral, and posterior. The actual luminal area was calculated from the diameter measurements obtained with the calipers using the formula for the area of an ellipse, i.e. $A = \pi \cdot a \cdot b$, where a and b are the lengths of the semi-major and semi-minor axes, respectively.

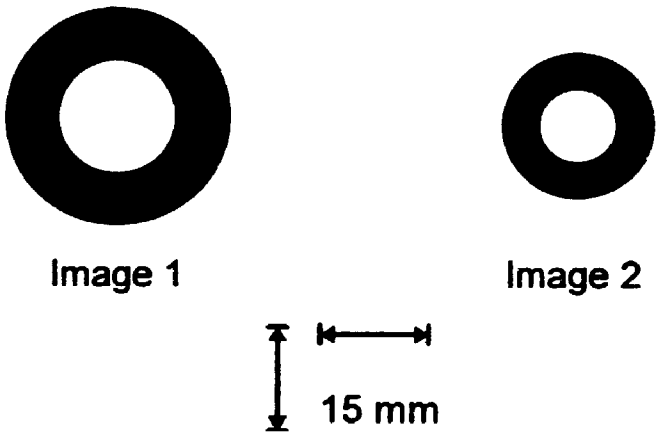

Figure 3.2 Schematic diagram of the calibration washers used to calibrate imaging system.

3.3 Results

3.3.1 System calibration

The accuracy of luminal area measurements was examined for washers similar to those shown in Figure 3.2. The measured luminal area was overestimated for both images when compared to the true luminal area: +4.4 ± 0.2% (S.E.M.) for Image 1, and +3.6 ± 0.3% for Image 2. However, these small differences from the true area were considered to be insignificant.

Mean washer wall thickness was calculated from measurements obtained from four locations for both of Images 1 and 2: top, bottom, left and right. These measurements were compared with the true value using a paired t-test. The values reported by the software underestimated the wall thickness of both images examined: -3.7 ± 0.3% for Image 1 and -2.5 ± 0.4% for Image 2. Although there was a discrepancy between the values reported by the two methods, these differences were not statistically significant (p=0.110, image 1; p=0.565, image 2). As a result, the methods were considered to give the same result.

3.3.2 Branch angle and parent area

No significant difference was present between the left and right branch angles (p=0.20). The mean left branch angle was 15.3 ± 2.4° (S.E.M.) while the right branch angle was 11.9 ± 1.9°. Table 3.2 summarizes the branch angles measured from the 14 aorto-iliacs studied. The total branch angle, defined as the sum of left and right branch angles, was independent of patient age.

The parent luminal area was measured from the slice through the parent branch that was furthest from the apex. In the youngest patients studied (< 1 year), no difference was observed in parent areas measured between patients. With an increase in age, the parent area increased non-linearly until a plateau was reached around the fifth decade (Figure 3.3). The relationship between parent area and age

Table 3.2 Summary of parent area and both left and right branch angles.

Patient age (yrs)	Parent area (mm^2)	Branch Angle (degrees)		
		Left	Right	Difference
0.003	11.3	5.7	4.8	+0.9
0.25	13.2	23.3	19.9	+3.4
0.75	8.6	33.9	24.6	+9.3
0.92	7.5	19.9	16.7	+2.2
6	51.5	13.1	8.6	+4.5
14	41.9	16.0	17.1	-1.1
19	98.5	16.0	13.4	+2.6
29	107.5	6.9	3.2	+3.7
41	141.0	9.9	7.3	+2.6
44	122.7	7.6	7.6	0
59	141.0	25.1	17.4	+7.7
61	143.1	25.2	5.9	+19.3
73	176.7	9.2	2.0	+7.2
76	126.7	9.0	17.4	-8.4
Average	85.1	15.3	11.9	+4.4
(±S.E.M.)	16.7	2.4	1.9	1.7

Parent area was measured in the section that was the furthest distance from the apex. No correlation was present between parent area and total branch angle. No significant difference was found between the magnitude of left and right branch angles ($P=0.20$).

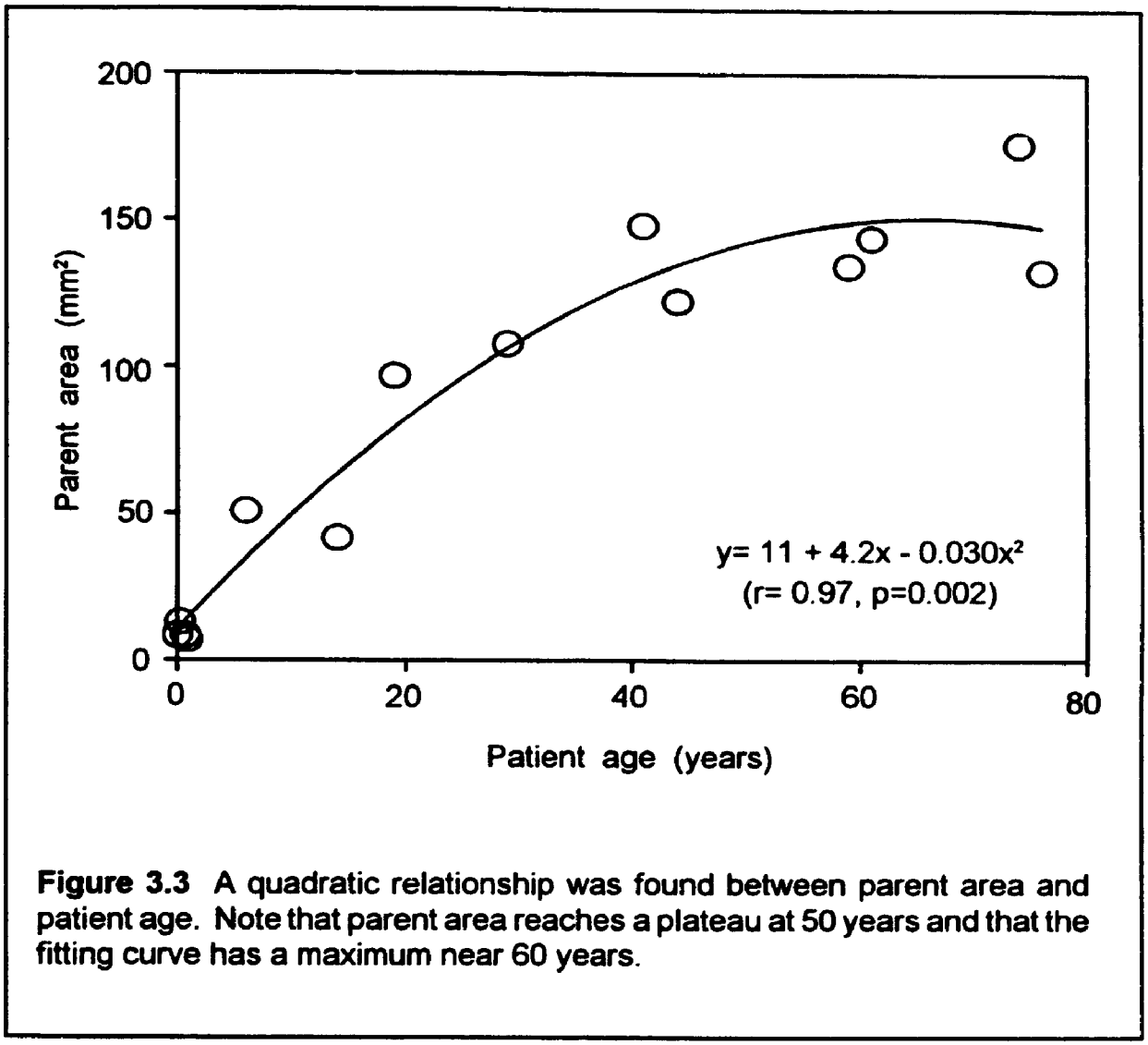

Figure 3.3 A quadratic relationship was found between parent area and patient age. Note that parent area reaches a plateau at 50 years and that the fitting curve has a maximum near 60 years.

was described with a quadratic function ($r=0.97$, $p=0.002$). No correlation was found between parent area and total branch angle ($r=0.37$; $p>0.05$).

3.3.3 Area Ratio.

Area ratio was defined as the ratio of the summed daughter area to the parent area with each of the measurements taken one parent-tube diameter both proximal and distal to the apex of the bifurcation. Note that the parent area used to calculate area ratio was not the same value reported in section 3.3.2. Three arteries were excluded from this analysis since their daughter branches were less than one parent-tube diameter in length. The excluded samples were: V113_92, V108_92 and A111_91. The mean area ratio of the aorto-iliac bifurcation was 1.0 (±0.1). The area ratio decreased non-linearly from a maximum value of 1.4 (at 3 months) to 0.8 (at 76 years). The curve of best fit was a quadratic function ($r=0.98$, $p=0.013$, Figure 3.4).

3.3.4 Luminal cross-sectional area variation

Three large, linear changes in luminal area were measured in the human aorto-iliac bifurcation. Proximal to the apex, luminal cross-sectional area increased, then decreased to the apex and then increased in the daughter branches. As a result, the bifurcation was divided into three regions: pre-apical, apical and post-apical (Table 3.3). The pre-apical region, situated in the parent branch, increased in luminal area by 24.6% (±3.9% S.E.M.). Luminal area in the apical region decreased by 21.2% (±3.1% S.E.M.) and corresponded to the region closest to the apex of the bifurcation. The post-apical region was situated distal to the apex and increased in luminal area by 12.4 ± 3.4% (S.E.M.). An analysis of variance followed by a Pairwise Multiple Comparison showed that the magnitudes of the area changes in the pre-apical and post-apical regions were significantly different ($p<0.05$).

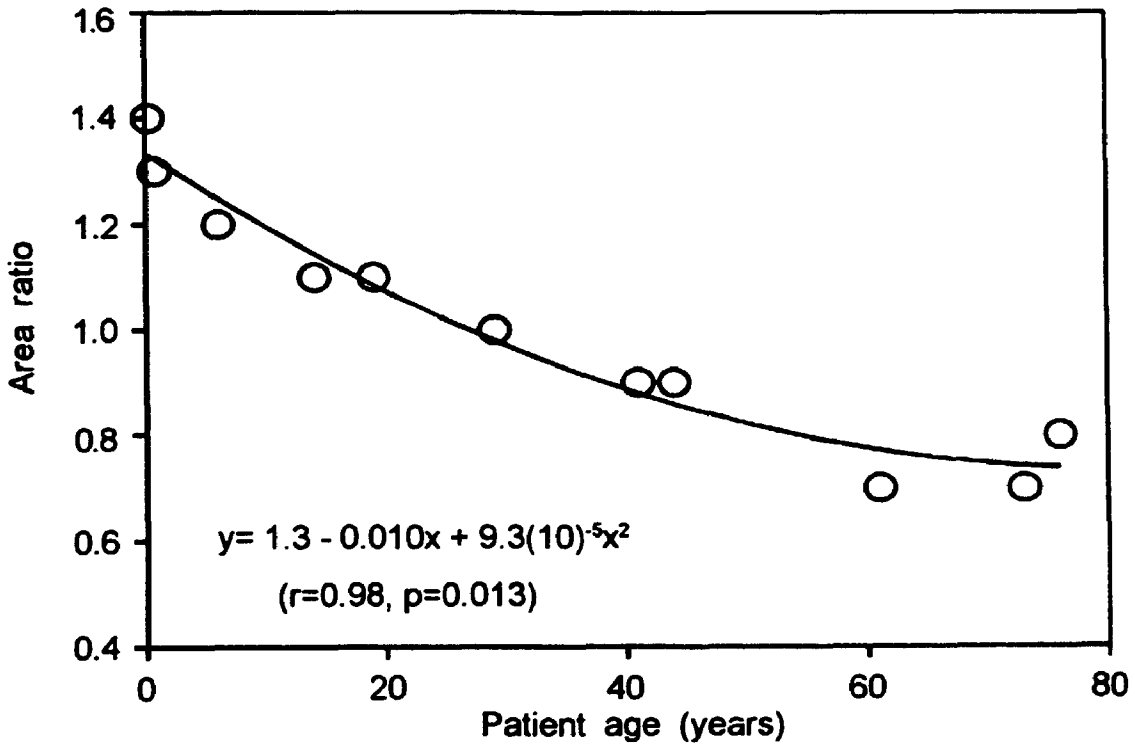

Figure 3.4 Area ratio was defined as the ratio of the summed daughter area to the parent area measured one parent-tube diameter from the apex. A quadratic function was used to fit the relationship between area ratio and age. Note that the area ratio reached a minimum value of 0.8 in the sixth decade. Three arteries were excluded from this analysis since their daughter branches were less than one parent-tube diameter in length.

Table 3.3 Summary of luminal cross-sectional area variation in the human aorto-iliac bifurcation.

		Area change (%)		
Autopsy number	Patient age (yrs)	Pre-apical	Apical	Post-apical
V113_92	0.003	+69.3	-19.2	+6.4
V89_92	0.25	+29.8	-18.2	+37.1
V100_92	0.75	+32.6	-45.6	+31.5
V108_92	0.92	+17.8	-11.6	+26.4
V87_92	6	+18.5	-8.7	+8.8
V161_92	14	+22.2	-13.5	+6.1
A99_92	19	+19.5	-6.0	+16.9
A42_92	29	+13.9	-22.9	--
A84_92	41	+16.2	-28.9	+3.7
A31_92	44	+18.5	-16.5	+3.0
A111_91	59	+29.8	-9.9	+4.7
A53_92	61	+11.1	-30.0	+12.5
A71_92	73	+16.5	-37.7	+3.1
A129_91	76	+28.8	-27.8	+3.9
Average	30.3	+24.6	-21.2	+12.4
(±S.E.M.)	7.9	3.9	3.1	3.4

The aorto-iliac bifurcation was divided into three regions: pre-apical, apical and post-apical. Large changes in luminal area were observed in each of these regions. Positive changes represent an increase in cross-sectional luminal area.

No correlation was found between the magnitude of the area change in the pre-apical region and age ($p=0.054$). However, luminal area in the apical region tended to increase linearly with an increase in age ($r=0.75$, $p=0.002$) while, post-apical area tended to decrease as age increased ($r= 0.665$, $p=0.013$).

I have shown previously (section 2.3.1) that two area changes were present in both porcine renal and human cerebral bifurcations. The presence of three distinct regions of luminal area variation in the human aorta made it impossible to compare the magnitudes of these area changes between groups, and suggest that the two types of bifurcations are quite different.

3.3.5 Luminal area offset

Luminal area offset was defined as the distance from the apex of the bifurcation to the location of the maximum cross-sectional area. The mean area offset was 5.1 ± 1.5 (S.E.M.) parent tube diameters upstream from the bifurcation apex, i.e. in the parent branch. All of the vessels studied, with one exception, had the maximum luminal area in the parent branch. The one exception had the maximum area at the apex. This result is quite different from the porcine renal bifurcation where I showed that the maximum area was always at the apex of the bifurcation (see section 2.3.1). This means that in the aorto-iliac bifurcation, in contrast to the muscular bifurcations where the mean velocity is lowest at the apex and the flow decelerates toward the flow divider, in the aorta flow accelerates towards to the flow divider and then decelerates in the daughter branches.

3.3.6 Area taper

Area taper was defined previously (see section 2.3.2) as the change in luminal cross-sectional area divided by the distance over which that change occurred. Since the magnitude of luminal area changes reported above depend on the length

of the vessel studied, taper provides a normalized representation of area changes. Three area tapers were calculated corresponding to the three area changes presented above, namely, pre-apical, apical and post-apical. Positive taper corresponded to a narrowing (with an acceleration of flow) while negative taper represented an expansion or flaring region (causing flow to decelerate). The mean area taper in the pre-apical region was -0.7 ± 0.1mm (S.E.M.), +2.44 ± 0.73mm in the apical region and -1.09 ± 0.29mm in the post-apical region.

A one way ANOVA followed by a Pairwise Multiple Comparison found a statistically significant difference in the magnitude of the area taper in the apical versus post-apical region ($p<0.05$) and in the apical region versus pre-apical region ($p<0.05$). No difference was found between the magnitudes of the taper in the pre-apical and post-apical regions ($p>0.05$).

Taper in the apical region tended to increase linearly as age increased ($r=0.65$, $p=0.012$). No such relationship was found between age and the tapers in the pre-apical ($r=0.39$, $p=0.165$) and post-apical regions ($r=0.263$, $p=0.386$), respectively.

3.3.7 Wall thickness variation in the parent branch

In order to determine if wall thickness was constant around the lumen, and as a function of distance along the aorta, variations in the cross-sectional wall thickness of the parent branch were measured using a polar grid that was centred on the centroid of the lumen. Measurements were recorded in fifteen degree increments from every fortieth section (i.e. every 400μm).

Figure 3.5 shows the circumferential variation in wall thickness measured in four of the ten samples studied: 1 day, 9 month, 19 year and 41 year. Each data point represents an average (±S.E.M.) wall thickness measured along the parent branch. Anterior and posterior wall thickness were defined at the surface closest to the intestine and the spine, respectively. Two maxima and two minima were present

in each of these patients except in the 1 day (i.e. 0.003 yrs) old patient where wall thickness was minimum posteriorly and uniform elsewhere, and in the 3 month (i.e. 0.25 yrs) old patient where wall thickness was uniform everywhere. In the remaining patients, minima were present both anteriorly and posteriorly (towards the spine) while the lateral positions corresponded to the sites of maximum wall thickness. Table 3.4 summarizes the variation in wall thickness measured laterally as well as in both anterior and posterior directions. Wall thickness variations were not measured in the five samples that were decalcified because the decalcifying process solubilized calcium that would have included in thickness measurements. In the remaining arteries, no correlation was found between the average wall thickness and patient age; however, a linear relationship was found between the left-lateral and right-lateral wall thicknesses (Figure 3.6, $r=0.866$, $p=0.003$). A similar relationship was found between the anterior and posterior wall thickness ($r=0.834$, $p=0.013$). This implies that the aorta is not isotropic around its circumference, but is probably similar about axes drawn through the center either in the lateral or antero-posterior direction.

Changes in wall thickness along the length of the parent branch are shown in Figure 3.7. Each of the data points represents the average thickness (± S.E.M.) from 0° to 345°. In both the 1 day old and the 9 month old patients, there was no correlation between sample length and wall thickness. However, in each of the older patients, the parent branch was thickest furthest from the apex of the bifurcation and became thinner towards the apex.

No correlation was found between average wall thickness and luminal radius along the parent branch ($p>0.05$).

The wall thickness measurements are relevant for calculating wall tensile stress. However, they may also reflect remodelling of the wall as Glagov has suggested that the artery wall remodels in order to maintain a shear rate of $1.5 N/m^2$.

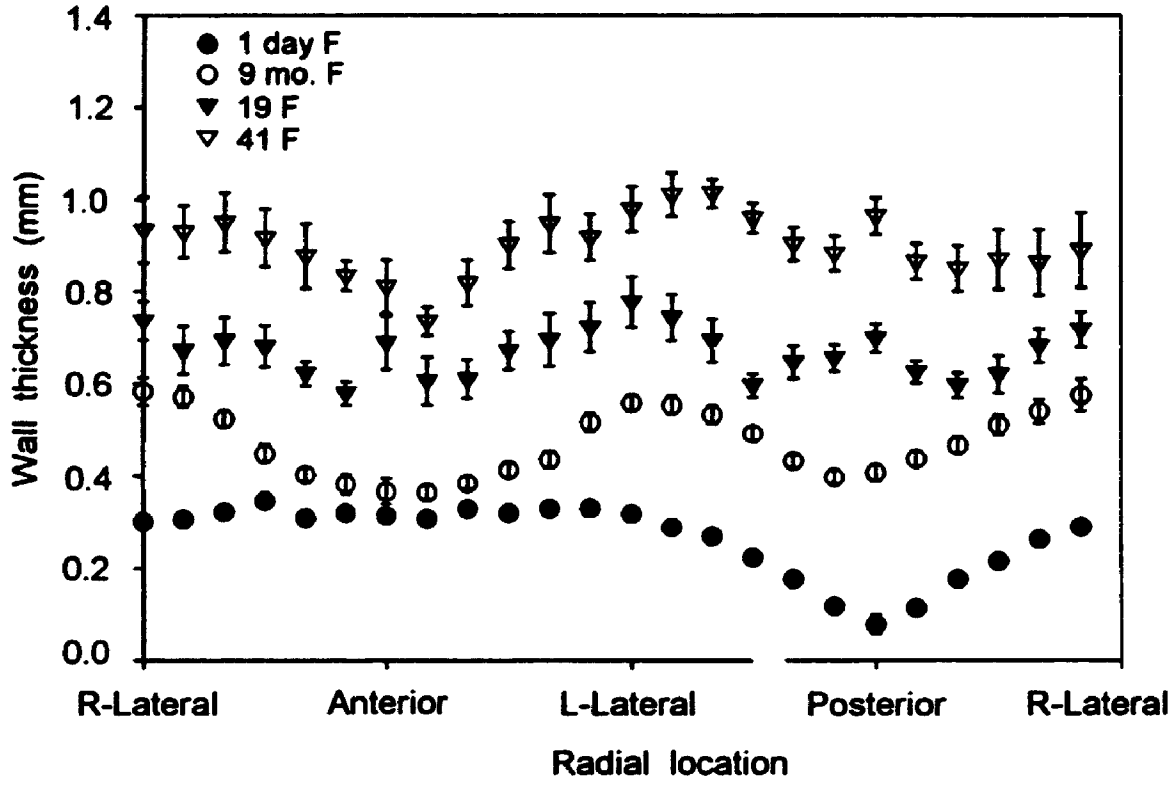

Figure 3.5 Circumferential variation in parent wall thickness was examined in fifteen degree increments. Two minimina and two maxima were found in all patients except in the one day old where only one minimum was found.

Table 3.4 Summary of wall thickness variation measured in lateral, anterior and posterior directions.

Patient age (years)	Polar angle				Average thickness (mm)
	R-lateral	Anterior	L-lateral	Posterior	
0.003	0.30	0.32	0.32	0.08	0.25
0.25	0.42	0.42	0.42	0.42	0.42
0.75	0.58	0.37	0.56	0.41	0.48
0.92	0.79	0.85	0.85	0.72	0.82
6	0.29	0.26	0.31	0.28	0.28
14	0.40	0.36	0.46	0.54	0.43
19	0.93	0.81	0.98	0.96	0.90
41	0.74	0.69	0.78	0.70	0.67
44	0.74	0.72	0.75	1.0	0.76
Average	0.58	0.53	0.60	0.57	0.56
(±SEM)	0.08	0.08	0.09	0.11	0.08

Note: Wall thickness variations were not measured in the five samples that were decalcified because the decalcifying process solubilized calcium that would have been included in these thickness measurements.

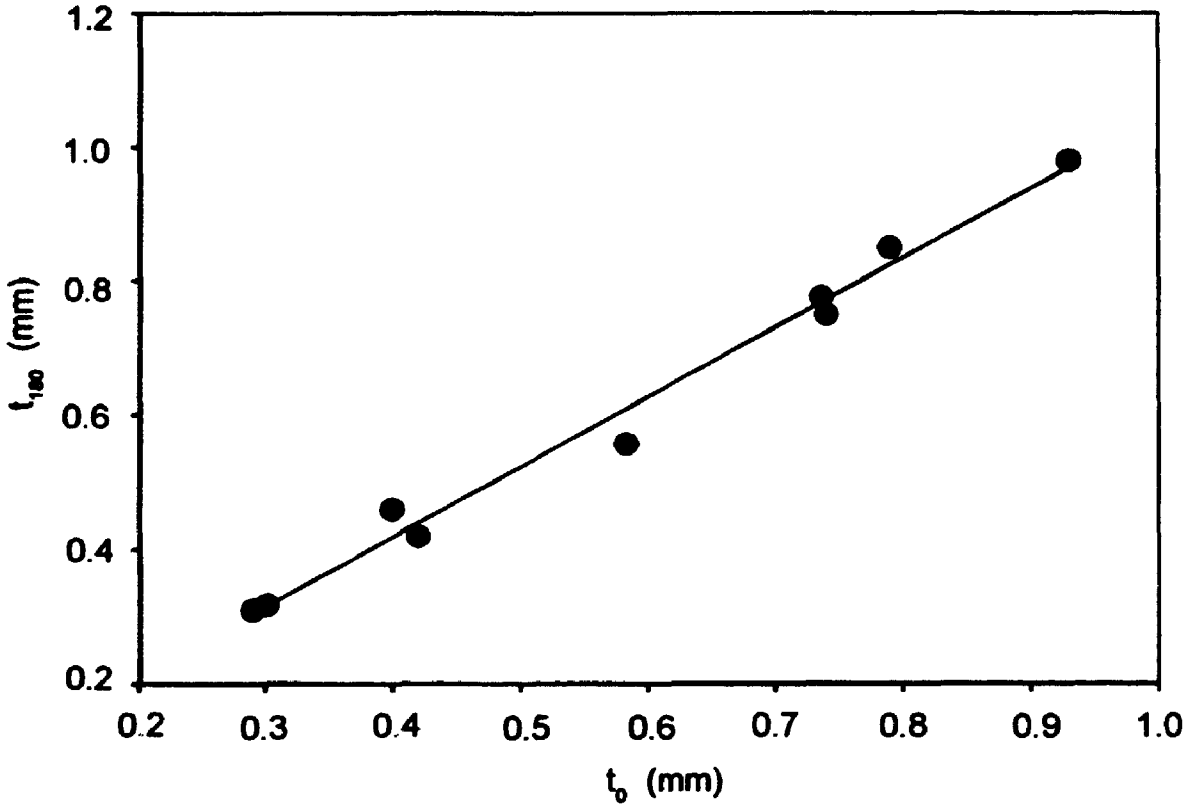

Figure 3.6 A linear relationship was found between the average thickness at left-lateral (i.e. 180°) and right-lateral (0°) from each of the nine patients examined ($r=0.994$, $P<0.001$). Although not shown here, a linear relationship was also present between the anterior and posterior thicknesses. These data imply that aortic wall thickness is similar about axes drawn through the center either in the lateral or antero-posterior direction.

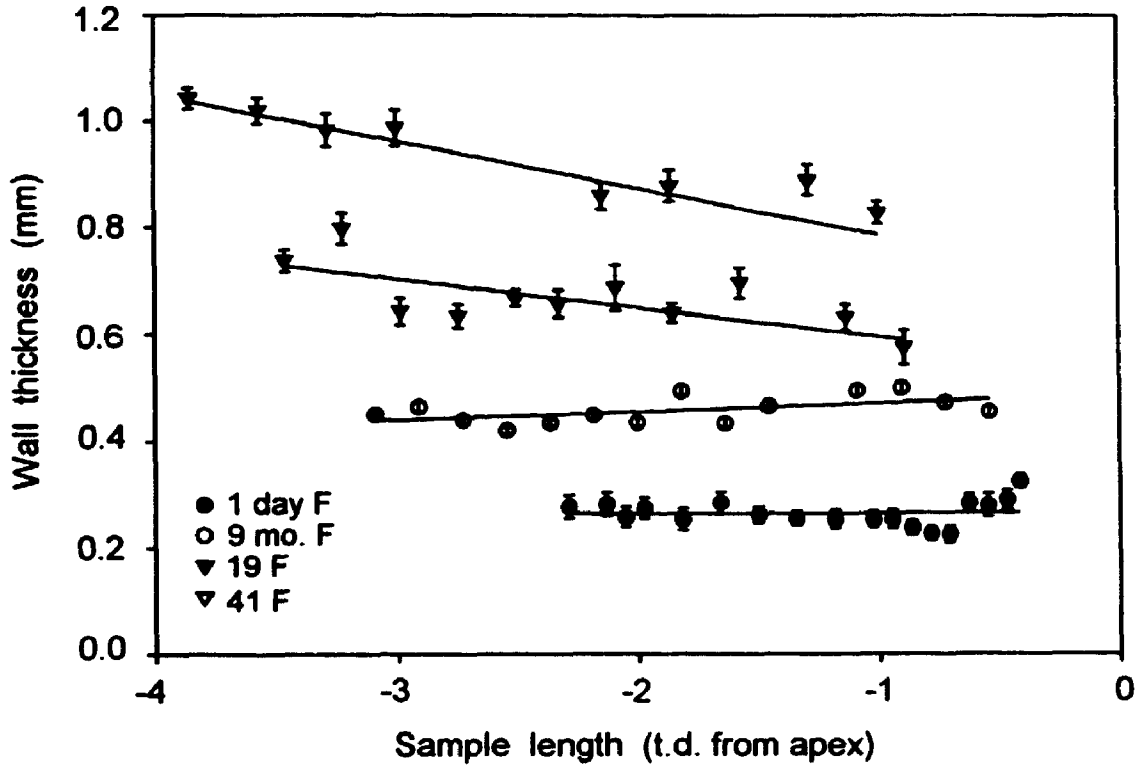

Figure 3.7 Longitudinal variation in cross-sectional wall thickness of the parent branch. Each point represents the average thickness from 0 to 345 degrees from each section. (t.d. = parent tube diameters).

The fact that the lateral region is thicker supports my observation that the aorta flares to the sides to form branches. The fact that the antero-posterior wall are thinner fit the diameter taper seen in that direction. Thus, this data supports Glagov's proposal that the wall remodels in response to luminal shear stress. To show this conclusively, it would be necessary to measure the velocity profiles in these regions. Since nobody has measured the elastic response to pressure waves in local regions of the wall, it is not possible to say how this remodelling alters the tensile stress in the lateral walls as opposed to the antero-posterior ones. I would predict that there will be differences in tensile stress and that these differences will be age-dependent.

3.4 Conclusions

I have developed a method to measure both luminal cross-sectional area and wall thickness from serial sections of the human aorto-iliac bifurcation. The error attributed to video recording, digitizing and measuring luminal area and wall thickness of washers was < 5% and was considered to be negligible.

Branch angles were calculated from the x- co-ordinate of the centroid from each section through each daughter branch along the length of the bifurcation. No significant difference ($p>0.05$) was found between left and right branch angles: 15.3 ±2.4° (S.E.M.) and 11.9 ±1.9°, respectively. The mean total branch angle calculated from fourteen patients was 27.6± 4.0° and was consistent with branch angles of 35.0 ± 11.1° reported previously by Bargeron et al. (1986). This group measured *in situ* branch angle, angular asymmetry and flow divider offset from aortograms of seventy human aorto-iliac bifurcations that were obtained at autopsy and perfusion fixed at mean arterial pressure. The mean angular asymmetry (difference between left and right branch angles) was +4.4 ± 1.7° (S.E.M.) in the present study while Bargeron reported an angular asymmetry of -2.2 ± 19.8° (S.D.). The results of both studies suggest that the difference between left and right branch angles is negligible and

that the bifurcation is symmetrical about the parent axis.

Area ratio is a dimensionless parameter defined as the ratio of the summed luminal area of both daughter branches to that of the parent branch measured one parent-tube diameter either side of the apex. A quadratic relationship was found between area ratio and patient age. The largest area ratio was found in the youngest patients. Area ratio decreased with age and plateaued near a value of 0.75 after the sixth decade. Gosling et al. (1971) studied the area ratio from three human cadavers and 88 aortograms from patients 0 to 50 years. They showed that the area ratio decreased linearly from an optimum value of 1.11 in the first decade to 0.75 by the fifth decade. As discussed in section 2.3.2, I do not believe that the area ratio is as valid a hemodynamic parameter as the area taper. In addition, the variablility of the offset (i.e. the location of maximum cross-sectional area) could alter the area ratio dramatically.

Several studies have used aortography to examine bifurcation geometry (Gosling et al., 1971; Lee et al., 1982; Hoogendam et al., 1984). Aortography is advantageous compared to the sectioning technique that I have reported here since aortographic measurements are obtained *in vivo*, with proper tethering and under physiological conditions. As compared with the fourteen patients that I have studied with serial sectioning, aortographic-based studies have examined hundreds of patients. Although aortography is probably valid for measuring branch angles, this technique only provides a 2D cross-sectional view of the aorta which is likely elliptical near the apex of the bifurcation. As a result, area ratios reported previously were calculated by measuring luminal diameters and assuming that the aorta is circular in cross-section. Chapter 4 looks at the likely errors in assuming cross-sectional circularity.

Luminal area changes reported previously for the porcine renal bifurcation (see Chapter 2.3.1) showed that there were two unique regions in the bifurcation: an

increase in luminal area up to the bifurcation followed by a decrease in area into the daughter branches with the maximum area at the apex. In the human aorto-iliac bifurcation, three regions with large changes in luminal area were identified and defined as: pre-apical, apical and post-apical (or daughters). Luminal area increased along the pre-apical region, then decreased in the apical region and increased into the post-apical region. With one exception, the maximum luminal area was always proximal to the apex of the flow divider while in one case the maximum was at the flow divider. A positive, linear correlation was found between area changes in the apical region and age, while a negative, linear correlation was present between post-apical area and age. The geometry of the pre-apical and apical regions suggest that there is a bulge, or bulbous-type expansion proximal to the flow divider in all of the patients studied. This was not observed in the porcine renal bifurcation, and to my knowledge, has not been described previously. It remains unclear what function this bulge serves in the bifurcation.

Three area tapers were calculated in this study corresponding to each of the three area changes reported above: pre-apical, apical and post-apical. The magnitude of the taper from each region was significantly different from zero, while taper in the apical region was significantly different in magnitude from taper present in the pre- and post-apical regions.

The aortic wall thickness was greatest at the lateral positions of older patients while the thinnest regions corresponded to both anterior and posterior locations. In the youngest patient studied (1 day), the parent trunk was extremely thin posteriorly and uniform elsewhere. The next youngest arterial specimen, a 3 month old, showed no variation in wall thickness around the circumference or along the parent branch while the rest of the patients studied showed the same trend as I have described for the oldest patient, i.e. thickest laterally and thinnest both anteriorly and posteriorly. More samples would have to be studied to show a statistically significant

trend. In older patients, the analysis is complicated by thickening due to atherosclerosis.

It has been well documented that arterial wall thickness changes with age due to several factors, of which, atherosclerosis and hypertension have been studied in greatest detail. No detailed studies of the location of these lesions around the lumen have been done to my knowledge. In older patients, atherosclerotic lesions tend to develop in the lateral regions of the bifurcation that correspond to the locations that I have reported as being thickest in cross-section. Hypertension acts to increase wall thickness by increasing either the size of smooth muscle cells present in the tunica media (this process is defined as hypertrophy), or by increasing the number of individual smooth muscle cells already present in the media (defined as hyperplasia). Although the histories of the patients from which tissue was collected did not indicate that the patients were hypertensive, the effect of hypertension on wall thicknesses reported in this study are likely small. Furthermore, hypertension would probably alter medial thickness uniformly around the circumference; however, this remains to be proved.

In summary, the results of this study have shown that:

(1) the aorto-iliac bifurcation branches symmetrically, and that branch angles were not correlated with patient age,

(2) there are three large changes in luminal area at the aorto-iliac bifurcation and the largest cross-sectional area was proximal to the flow divider,

(3) there are also three distinct tapers in this bifurcation. The hemodynamic inferences are as follows: proximal to the flow divider, blood flow decelerates in the flaring region and could form a separation zone. Low shear stress associated with separation zones is a known risk factor in the localization of atherosclerotic lesions.

(4) parent vessel area increased non-linearly with age and plateaued at 50

years. This suggests that initially, the aorta grows with the person until it reaches a certain size; however, its' gradual and continuing growth after whole body maturation has no explanation.

(5) area ratio decreased non-linearly from a maximum value of 1.4 (at 3 months) to 0.8 (at 76 years). The area ratio is not a good parameter to describe the geometry of the aorto-iliac bifurcation since the variability of the offset could alter the area ratio dramatically.

(6) cross-sectional wall thickness was greatest laterally while the anterior and posterior regions were thin. In one of the adult samples studied, the right-lateral wall thickness was 0.74 mm while the posterior wall was 1.0 mm thick. This implies that the aortic wall is anisotropic and so Laplace's law should be used only to calculate local wall tension.

Based on the results of this study, the geometry of the human aorto-iliac which is an elastic artery bifurcation is different from the geometry observed in the muscular Y-bifurcations. To my knowledge, this has not been demonstrated previously.

While it is easy to predict that mean flow velocity will be lowest at the apex and highest at the flow divider, it is harder to predict the velocity profile, and to delineate the location of separation zones. We are collaborating with Dr. M. Nakamura of Akita University in Japan to do this (see section 6.2.3)

The variations in luminal geometry measured at Y-bifurcations have ignored changes in luminal shape that occur at the apex due to the formation of the flow divider. Shape changes at the bifurcation have also been ignored in studies that have compared bifurcations using area ratios (Gosling et al., 1971; Lee et al., 1982; Hoogendam et al., 1984) and in studies that have examined bifurcation geometry (Bargeron et al., 1986). In the following Chapter, I have examined shape changes

measured in both the porcine renal and the human aorto-iliac bifurcations that were studied in Chapters 2 and 3. These shape changes will help us to predict how the velocity profile might change over the region proximal to the flow divider.

Chapter 4

Shape changes proximal to the apex of Y-bifurcations in arteries[1].

The geometrical studies that I have reported in Chapters 2 and 3 have examined taper at Y-bifurcations of both porcine renal and human aorto-iliac bifurcations as well as changes in wall thickness at the aorto-iliac bifurcation. In this study, I have examined 3D, luminal shape changes proximal to the apices of both human aorto-iliac and porcine renal bifurcations that were pressure-fixed at mean arterial blood pressure. Area changes are used to predict whether mean velocity will increase or decrease, while shape changes will suggest how the velocity profile might vary.

4.1 Introduction

Previous studies have shown that both bifurcation geometry and hemodynamic forces such as shear stress are important factors in the localization of atherosclerotic lesions (Fry, 1968; Caro et al., 1971). In Chapters 2 and 3, I have reported large changes in luminal cross-sectional area both proximal and distal to the apex of both porcine renal and human aorto-iliac bifurcations while Macfarlane (1985) has reported similar measurements from human cerebral bifurcations. These large changes in luminal area likely alter both blood flow velocity and blood flow patterns through the bifurcation region and may be involved in the localization of atherosclerotic lesions within the bifurcation region. The geometrical studies of the aorto-iliac bifurcation that have been reported previously (Gosling et al., 1971; Bargeron et al.,

---

[1]Segments of this chapter have been published in: Frontiers of Medical and Biological Engineering (vol 5, No 2, pp127-133, 1993). This study was reproduced with permission from VSP. Dr. Roach and I are co-authors. In this study, I was responsible for data collection and analysis, preparation of tables and figures and for writing the initial draft of this manuscript.

1986), including the studies that I have presented in Chapter 3, have ignored changes in the shape of the aorta proximal to the apex of the bifurcation.

Bifurcations are formed by expanding a circular parent trunk in the lateral directions while pinching-in from the antero-posterior direction simultaneously (Figure 4.1). This produces a 'saddle' with two radii of curvature at the apex: the curvature in the plane of the bifurcation (external apical curvature) and the curvature in the plane perpendicular to the bifurcation (internal apical curvature). This changes the shape of the aorta from being circular, to elliptical and then to an hour-glass in cross-section at the apex. Macfarlane et al. (1983a) examined shape changes at the apex of isolated human cerebral bifurcations with changes in transmural pressure and showed that there were large changes in the internal curvature (curvature perpendicular to the plane of the bifurcation) but remarkably little change in the curvature in the plane of the bifurcation over the same range of transmural pressures. Macfarlane suggested that as the internal curvature flattens, the arterial wall becomes thinner and apical wall stress must increase. Unfortunately, changes in wall thickness near the apical region are difficult to measure with the techniques that I have developed to examine wall thickness variations proximal to the apex (see Chapter 3.3.6). Longitudinal sections would be more appropriate for this.

In this study, I have examined the shape changes that occur proximal to the apex of both the porcine renal and the human aorto-iliac bifurcations and I have attempted to relate these shape changes to the variations in luminal cross-sectional area that I have reported in the preceding chapters.

4.2 Methods

Bifurcations were obtained from two locations, the human aorto-iliac junction (Chapter 3) and the porcine renal bifurcation (Chapter 2). These are the same

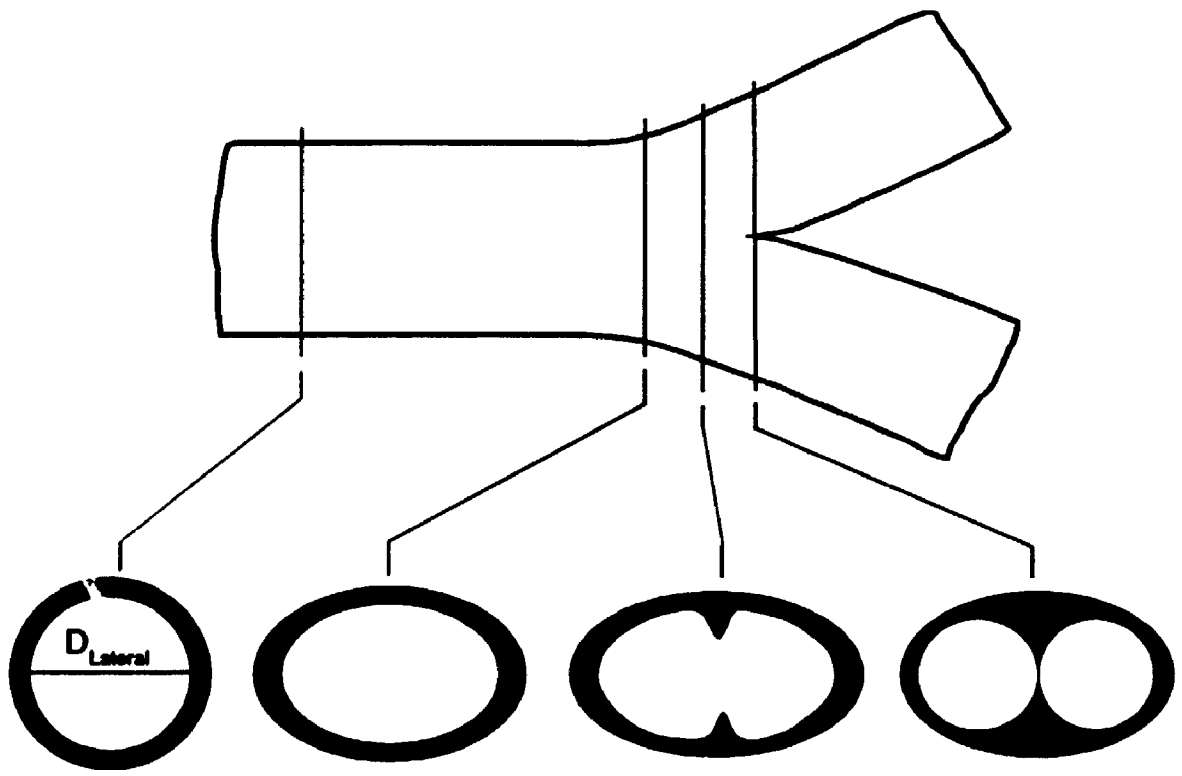

Figure 4.1 Schematic diagram of an arterial Y-bifurcation. The apical region of a bifurcation is formed by expanding the parent branch in the lateral direction while pinching-in in the wall from the antero posterior direction. This transformation produces two circular daughter branches from one circular parent branch. Blood flow is from left to right.

vessels that were presented previously. Porcine renal bifurcations were harvested from two groups of pigs, an adult group (>52 weeks old) and a juvenile group (6-14 weeks old) while human aorto-iliacs were obtained from fourteen patients (age range = 1 day to 76 years). The method used to section, video record and digitize serial sections from these vessels has been described previously (see Chapters 2.2 and 3.2); however, the analysis was different.

4.2.1 Analysis of parent shape

The luminal cross-sectional areas of the parent trunk, as well as the major and minor diameters of the parent were measured digitally using custom written software and a computer equipped with a frame grabber (Data Translation). The error attributed to video recording, digitizing and measuring luminal areas was <5% (see Chapter 3.3.1).

The shape of each of the parent branches was determined by measuring the ratio of antero-posterior (AP) to lateral diameters from each of the sections along the parent branch but proximal to the apex. The lateral diameter was defined as the largest diameter while the corresponding AP diameter was measured in the orthogonal direction. As a result, the shape factor was always ≤ 1. Circular cross-sections have a diameter ratio of 1 while any deviation from 1 corresponds to an elliptical cross-section. Near the apex, parent cross-sections become hour-glass shaped (see Figure 4.1); however, the AP diameter near the apex was measured at one location in the centre of the section.

4.3. Results

4.3.1. Area Changes

Two large changes in luminal area were reported in the porcine renal bifurcation, an increase proximal to the flow divider with the maximum cross-sectional area

at the apex of the bifurcation, followed by a decrease in summed luminal area of the daughter branches (see Section 2.3.1). No significant difference was found between the area changes reported from the adult and young porcine renals and so shape changes were not measured in the young porcine renals.

Three area changes were noted in the human aorto-iliac bifurcation, an increase in the pre-apical region, followed by a decrease in the apical region, and finally, an increase in summed luminal area in the daughter region (Section 3.3.4). In all but one patient, the maximum luminal area in the human aorto-iliac was always proximal to the bifurcation while the location of the maximum in one patient was at the apex. Both the area changes and the location of the maximum cross-sectional area of these two groups would suggest there is likely a difference in the shape of the parent trunk in these bifurcations. Table 4.1 summarizes the area changes measured from both young and old porcine renals and from human aorto-iliac bifurcations.

4.3.2. Shape changes proximal to a bifurcation

(i) *Porcine renal arterial bifurcations:* Diameter-ratios were calculated for the parent branch of the renal bifurcation and proximal to the flow divider. At the apex, the cross-sections were elliptical in contrast to being circular proximally. Figure 4.2 shows the variation of antero-posterior to lateral diameters from one of the old porcine renal bifurcations. Note that the diameter-ratio plateaus near a value of one (i.e. circular cross-section) one parent tube diameter from the apex. However, it should be noted that although the ratio approaches 1.0, it plateaus at a mean value of 0.87 indicating that the main renal artery is always slightly elliptical in cross-section proximal to the apex. A third-order polynomial was used to fit the relationship between diameter and distance from the apex (in tube diameters, $r=0.99$, $p<0.001$).

(ii) *Human aorto-iliac bifurcations:* The variation in diameter ratios from human

Table 4.1 Summary of luminal area changes proximal and distal to the apex of a Y-bifurcation. (mean ± S E.M.)

		Area Change (%)		
	Area Ratio	Pre-apical	Apical	Daughters
Young porcine renal	0.8±0.2	+35.5±7.6	--	-43.2±9.5
Old porcine renal	1.2±0.1	+45.7±10.5	--	-15.9±5.2
Human cerebral	--	+94.5±5.0	--	-36.9±4.0
Human aorto-iliac	1.1±0.1	+24.6±3.9	-21.2±3.1	+13.3±3.3

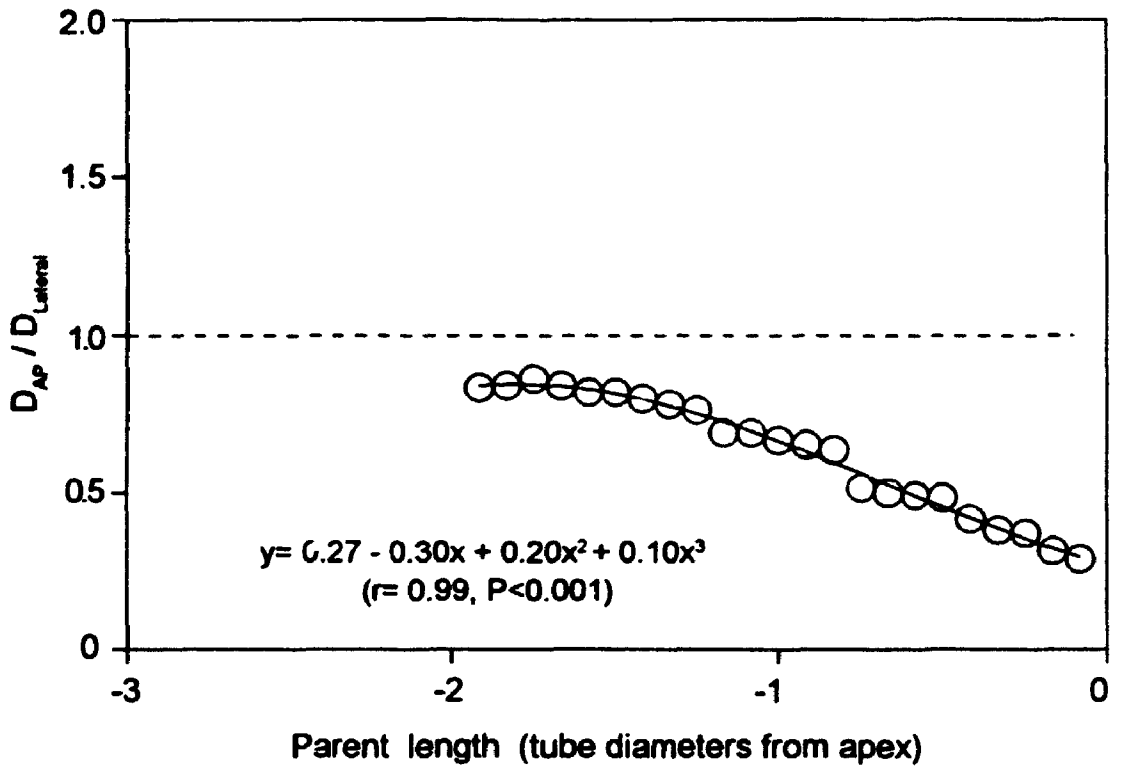

Figure 4.2 Change in diameter ratio as a function of distance from the apex in one of the old porcine renal bifurcations. The diameter ratio of old porcine renals plateaued near 1.0 (dashed line), one tube-diameter from the apex. The relationship between diameter ratio (i.e. shape) and parent length, fitted by computer analysis, was described best with a third order polynomial.

aorto-iliac bifurcations were very similar to those reported from the porcine renal artery. The diameter ratio was greatest at the maximum and decreased to a value near one over a very short distance from the apex (Figure 4.3). The human bifurcations were harvested from a wide age-group (from 1 day to 76 yrs); however, patient age did not have an effect on shape changes proximal to the aorto-iliac bifurcation.

4.4 Discussion

The results from this study suggest that certain geometrical paramaters of a Y-bifurcation may be invariant despite a large range in parent branch calibre; both the human aorto-iliac and the porcine renal were circular in cross-section away from the apex and both became more elliptical one parent-tube diameter from the apex. These shape changes were independent of age. All of the samples examined were pressure-fixed at mean physiological pressure and were limited to the region proximal to the apex of the bifurcation. The effects of pressure on the magnitude of the taper and the shape factors have not been measured. Macfarlane et al. (1983a) did show with optical methods that the internal apical curvature of human cerebral bifurcations flattened as pressure increased, while the external curvature changed very little. This implies that the bifurcation region does not respond uniformly to pressure. More detailed studies are required. There have been no studies of how taper changes with pressure. The values reported here are only for mean arterial pressure.

Stehbens (1974) examined both shape and luminal area changes in the rabbit aorta-iliac and canine aorto-iliac from serial sections of pressure-fixed arteries. He reported a distinct increase in luminal area proximal to the apex of the bifurcation with the greatest increase 1-2mm proximal to the apex. Stehbens suggested that the large increase in luminal area was due to the divergence of the lateral wall while

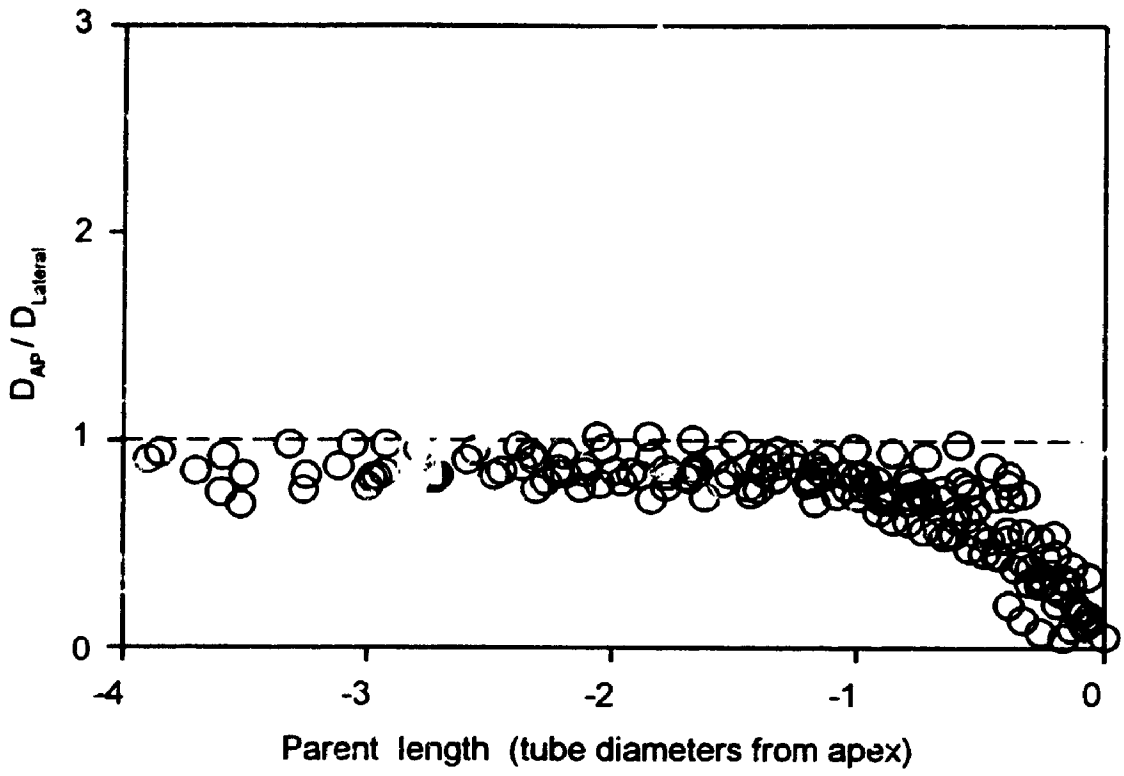

Figure 4.3 Variation in the ratio of antero-posterior to lateral diameter measured in twelve of the fourteen human patients as a function of distance from the apex (in tube diameters). Note that there is considerable overlap between samples; furthermore, all samples reach a diameter ratio near 1.0 (dashed line), one-parent diameter from apex.

the antero-posterior walls moved towards each other near the apex. Since the diameters of these arteries were not reported, I am unable to compare the distance of these area changes to the measurements I have presented above.

The shape changes that I have measured under static pressure conditions could have important implications for flow patterns near the bifurcation. Furthermore, the 3D changes in shape proximal to the apex have been ignored when luminal aortic geometry was examined from 2D aortograms (Gosling et al., 1971; Lee et al., 1982; Hoogendam et al., 1984). These parameters remain to be studied.

In summary, the results of this study have shown that:

(1) luminal area changes near the apex of Y-bifurcations occur in three-dimensions: lateral expansion and antero-posterior narrowing,

(2) the parent trunk is almost circular in cross-section away from the apex,

(3) the transition from circular to elliptical cross-sectional geometry occurred one parent tube diameter from the apex in all vessels studied, and,

(4) the shape of the parent branch was independent of patient/animal age.

The implications of these results are:

(1) 3D flow patterns in Y-bifurcations are needed since previous studies done in the central plane will miss important information

(2) Flow in the region of the abdominal aorta that develops aneurysms (i.e. renals to throat) is likely axisymmetric and the same in both the lateral and the antero-posterior directions while the region beyond this is asymmetrical

(3) Large changes in the ratio of AP to lateral diameters occur over short distances. This will result in large changes in the ratio of $d\tau/dl$ (i.e. change in shear stress per unit length). Differences in lateral and antero-posterior thickness suggest that the shape may change as a function of pressure.

(4) Since no change was measured with age, we can't use this to predict why older patients get atherosclerosis. We need to look at other parameters such as wall thickness or tensile stress as discussed in Chapter 3.

The studies presented in Chapters 2, 3 and 4 summarize the luminal geometry (taper and shape) and wall thickness measured from isolated, pressure-fixed arteries that were embedded and sectioned. The study presented in the following chapter examines *in vivo* changes in human aortic luminal geometry with the development of infrarenal aortic aneurysms.

Chapter 5

Changes in the geometry of the human aorta with the development of abdominal aortic aneurysms[1].

5.1 Introduction

The lower part of the abdominal aorta, from the renal arteries to the aortic bifurcation, is prone to develop both severe atherosclerosis and aneurysms. While the mortality from atherosclerotic disease of the coronary arteries and cerebral arteries is decreasing, the incidence of abdominal aortic aneurysms has increased almost three-fold in the last twenty years (Castelden et al., 1985; Fowkes et al., 1989; Reilly and Tilson, 1989). The reason for this increase is unknown, but has led to a suggestion that screening should be considered. This is particularly important when the mortality rates are considered. An untreated, ruptured aneurysm has a mortality of 100%, a surgically treated ruptured aneurysm has a mortality of 50%, while a surgically treated unruptured aneurysm has a mortality of 5% (Cole, 1989). Since aneurysms change the local geometry of the affected part of the aorta, we believe that geometrical parameters, as well as being related to the cause of the disease, may also play a role in screening for it.

Localized arterial disease is usually due to either local differences in flow or in elastic properties, or both. The disease, once present, may then cause other changes in flow or elastic properties. Both atherosclerosis and aneurysms tend to occur preferentially in the infrarenal abdominal aorta of humans. This region begins at the renal arteries and extends to the aorto-iliac bifurcation. This region of the

---

[1]This study has been accepted for publication as a book chapter, in: Recent Progress in Cardiovascular Mechanics: From basic research to clinical application (Editors: S. Hosida, T. Yaginuma, M. Sugawara, M.G. Taylor, and C.G. Caro). Dr. Roach and I are co-authors on this manuscript. I collected and analyzed the data, and I wrote the initial draft of the manuscript. (This chapter has not been published).

aorta has few branches other than small lumbar vessels that exit from the posterior surface of the aorta, and has been treated previously by several authors as a cylindrical segment. This study was designed to assess the geometry of this region in both normal aortas and in those with aneurysms.

The geometry of the lower abdominal aorta will determine, at least in part, both the flow patterns that are believed to play a role in atherogenesis (Caro et al., 1971; Hoogendam et al., 1984; Friedman ,1989; Mark et al., 1989) and also the mechanical properties. Studies that have used glass models showed that flow in all types of aneurysms was complex (Musto and Roach, 1980; Perktold, 1987), and included both vortex formation and turbulence. Both turbulence (Smith et al., 1970) and vortex formation (Goldsmith, 1974) predispose arteries to thrombosis. The geometry plays a role in the physical stresses that develop in the aortic wall (Gosling et al., 1971; Lallemand et al., 1972; Newman and Bowden, 1973; Lallemand et al., 1973). From the Law of Laplace, the circumferential tension equals the transmural pressure multiplied by the radius (Roach and Burton, 1957). Thus, if the radius increases under constant luminal pressure, the tension will rise. The aneurysm wall itself is likely thinned as the muscle and elastin are gone from the wall (He, 1992, p. 78). However, the role of thrombus in altering wall stress has not been determined. Theoretically, early thrombus should have little mechanical strength, but late organized thrombus that often contains collagen should be stronger. To my knowledge, this has not been investigated.

I have shown in pressure-fixed arteries that taper was present in both human cerebral arteries and in porcine renal arteries (Chapter 2). Since most abdominal aortic aneurysms develop in the region between the renals and the apex of the aorto-iliac bifurcation, the experiments reported here were designed to determine the geometry of this region.

Infrarenal aortic geometry was determined from aortograms and computed

tomographic (CT) images of the aortas of both normal patients and patients with infrarenal aortic aneurysms. Contrast aortography shows only the part of the lumen filled with dye and a 2D projection is taken in one plane, while CT shows cross-sectional views of the lumen and the outer circumference of the aorta. These studies were done at normal pressure and tethering since they are *in vivo* measurements.

5.2 Methods

5.2.1 Analysis of images from Computed Tomography (CT).

The aorta is clearly visible on CT films of the abdomen and lumbo-sacral spine, but we have measured only those where contrast was injected. Films obtained at University Hospital in London during the past year were chosen at random. These films are normally acquired at 1cm intervals longitudinally, and each image is averaged over a 5mm section thickness. The main advantage of this method is that a cross-sectional view of the aorta is obtained *in vivo* with normal tethering and at the blood pressure of the patient. It is impossible to know if the image was obtained during systole, diastole or a time-average representation of luminal geometry. Data from our laboratory (He, 1992, p. 71) showed that aneurysms were very stiff, and as a result, there is likely little difference between systolic and diastolic dimensions in patients with aneurysms. I hope to test this in the future with ultrasound.

These films were used to determine ellipticity along the aorta from the renals to the bifurcation. The longest diameter in each section was measured, as well as the diameter orthogonal to this. The ratio of the long axis to the short axis indicated the degree of ellipticity, and is 1.0 for a circle. Measurements in the bifurcation region were impossible because of the large interval between sections and the branch angle of the iliac arteries.

Studies were performed on 14 patients without aneurysms (normals) (mean age 59.9 ± 1.3 yrs, S.E.M.) and 9 patients with abdominal aortic aneurysms (mean

age 68.0 ± 1.1 yrs). Since contrast was used to outline the lumen, regions with thrombus were excluded.

The maximum diameter of the aneurysm was used to determine the relationship of lumen size to aneurysm size. The two are similar in the absence of thrombus, but can become different in large aneurysms that are particularly apt to contain large amounts of thrombus (Figure 5.1).

5.2.2 Analysis of aortograms from patients with and without aneurysms.

Only antero-posterior views were available (i.e. images acquired with patient on back and x-ray beam perpendicular to back). Thus, luminal area could not be measured unless circular symmetry was assumed. As will be shown below, this assumption is probably valid in the region upstream from the bifurcation. Films were examined from 8 patients without aneurysms (normals) (mean age 64.3 ± 2.5 yrs) and 9 patients with abdominal aortic aneurysms (mean age 69.4 ± 3.5 yrs) (Figure 5.2). Only patients that had contrast injections were included in this study.

The images were traced, and then the diameter measured with callipers at 1mm intervals from the renals to the aorto-iliac bifurcation. This longitudinal resolution would not be possible with CT slices that are acquired at 1cm intervals and 5mm in thickness.

5.2.3 Data analysis

5.2.3.1 Diameter change

This was obtained from the aortograms where only antero-posterior projections (giving the lateral diameter) were available, but measurements were made at 1mm intervals.

Diameter taper was defined as the difference in aortic diameter per unit length in the region of interest (i.e. from below the renals to just above the aorto-iliac

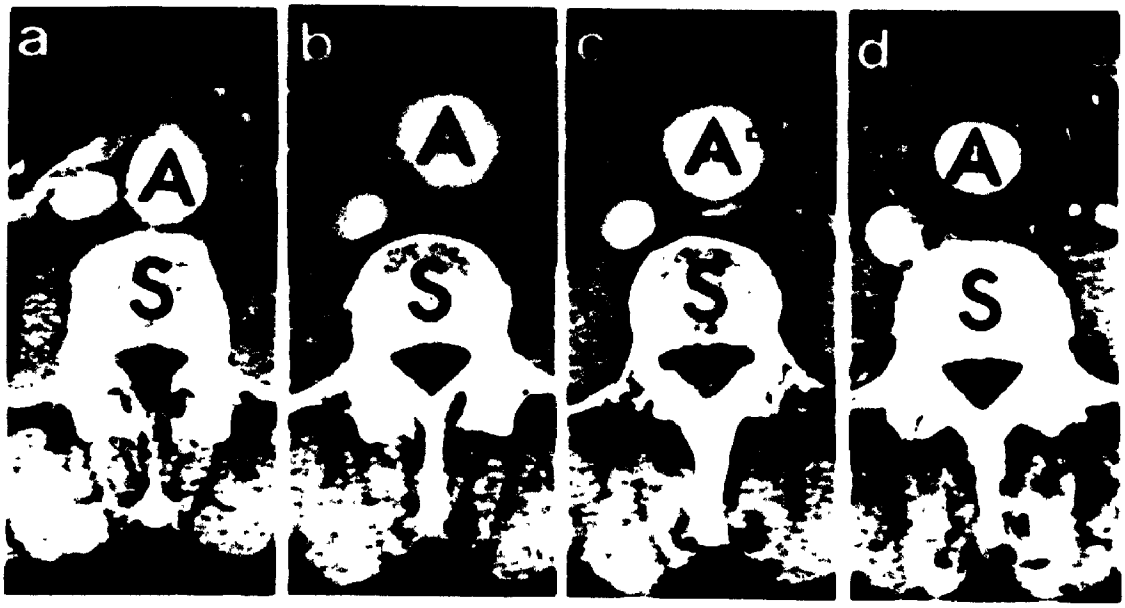

Figure 5.1 Sequential CT images showing the lumen (white) of the abdominal aorta (A) and the spine (S) from a 64 year female with an infrarenal aneurysm. Images (a) - (d) were obtained at: 150, 160, 170, and 180mm distal to the xiphisternum. (a) normal cross-section of the aorta. (b) marked enlargement in diameter relative to (a). Images (c) and (d) show continued aortic dilation and a reduction in luminal diameter due to thrombosis (grey). Calcification of the aorta is also visible (arrows).

Figure 5.2 Aortogram of a 71 yr female with an 'hour-glass' infrarenal aortic aneurysm (renal arteries marked with black arrow). Although hour-glass aneurysms were not included in this study, this aortogram is typical of the high-resolution images obtained with contrast aortography. Aortography only provides a map of blood flow since both thrombus and the wall of the aorta are absent in this image. Blood flow is from top to bottom.

bifurcation) and was measured from aortograms. Measurements were done only in the linear region. A **positive taper** implies the aorta is getting smaller (the normal situation) while a **negative taper** is equivalent to the flaring region seen in the proximal region of an aneurysm. This is a dimensionless parameter. Diameter taper and area taper are related where the lumen is circular (down to 1cm proximal to the flow divider) but not elsewhere.

5.2.3.2 Area change

Percent area change is a more important hemodynamic parameter than diameter taper as it will have a large effect on both average blood velocity and shear stress in that region. This can only be determined from isolated aortas (Chapter 3), and from the CT scans. Since the aortograms give only two-dimensional views, they provide only diameter, not area.

In previous studies (Chapters 2 and 3), I have measured area taper which is defined as the change in unit area per unit length and has units of mm. *In this chapter, I will use only diameter taper.*

5.2.3.3 Ellipticity

This is defined as the ratio of the long axis to the short axis of the aorta at any one location. An ellipticity of 1.0 implies the aorta is circular. These measurements were obtained from the CT scans, but could not be obtained from the aortograms. Note that my definition does not separate whether the long axis is in the antero-posterior direction, transverse direction or another direction.

5.2.3.4 Statistical analysis

A Mann-Whitney Rank Sum Test (Witte, 1989) was used to determine if the aorta was elliptical from the CT scans, and to determine if the tapers were different

in different regions. Linear regression analysis was used to determine the statistical significance of the relationship between parameters of the aneurysm and its lumen.

5.3 Results

5.3.1 Diameter taper from aortograms

In the normal aorta, positive taper was found from the renals to a region just upstream to the bifurcation that has been defined as the throat (Bargeron et al., 1986). Negative taper, flaring, was present between the throat and the apex of the aorto-iliac bifurcation. The largest cross-sectional area of the aneurysm was defined as the apex since a geometrical reference point was needed. Infrarenal aortic geometry is shown schematically in Figure 5.3. All tapers were significantly different from zero ($p<0.05$). The mean taper in the pre-throat region was +0.07 (±0.02 S.E.M.) and -0.63 (±0.06 S.E.M.) in the pre-apical region (Table 5.1). In patients with infrarenal aneurysms, the aorta flares in the proximal part of the aneurysm and then tapers to the throat, and then flares as before in the pre-apical region (Table 5.2). No significant difference was found between the magnitude of the taper from the throat to the apex of the normal patients and patients with an aneurysm ($p>0.05$).

5.3.2 Correlation of lumen and wall diameter in aneurysms by CT.

The dependence between luminal diameter and aneurysm diameter was found to be linear in the AP direction ($r=0.84$, $p<0.05$, Figure 5.4), but not in the lateral direction ($r=0.44$, $p>0.4$). The cross-sectional area of the lumen and the aneurysm was also linearly related ($r=0.82$, $p<0.05$, Figure 5.5); as are the diameter ratios (Figure 5.6, $r=0.93$, $p<0.05$).

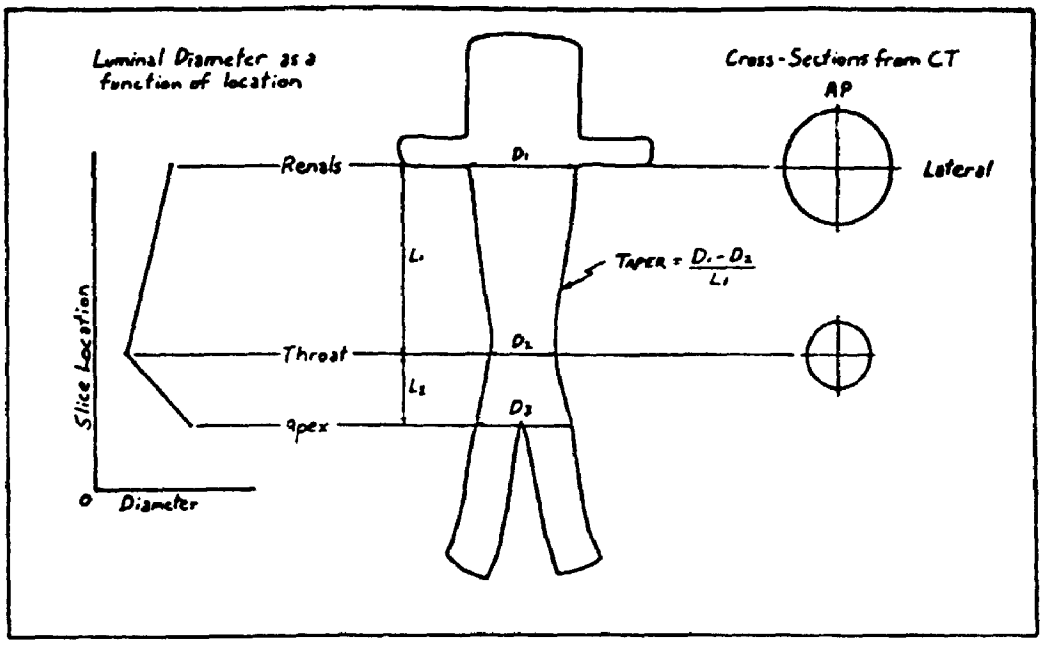

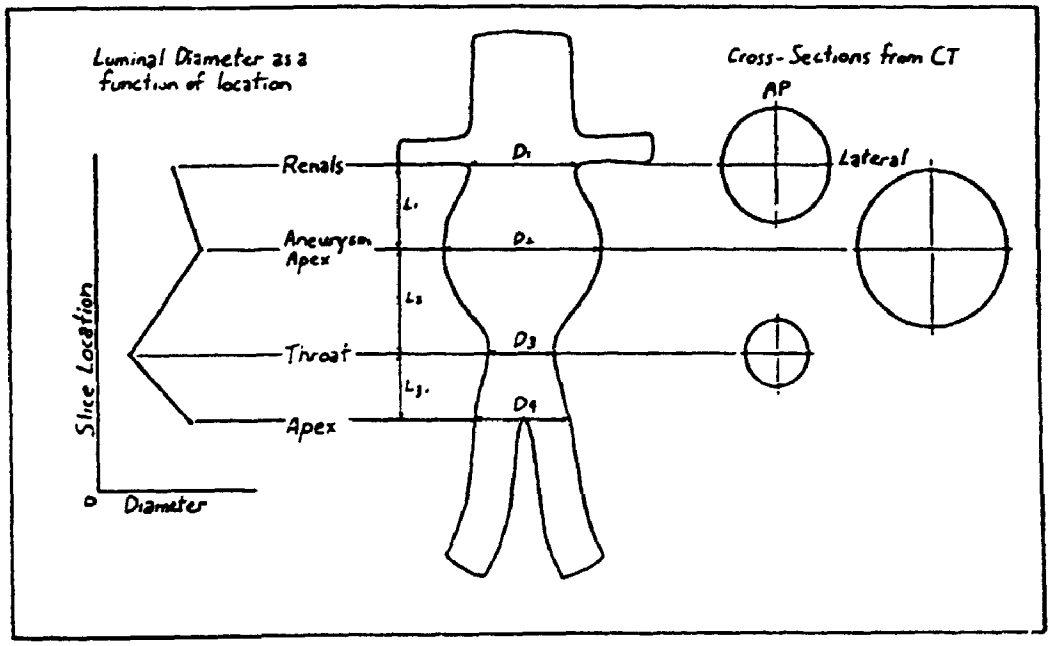

Figure 5.3 (above) Longitudinal variation in luminal diameter was examined from aortograms of normal patients. Diameter taper was calculated as the ratio of diameter change to the segment length over which the change occurred. Positive taper was present between the renals and the throat (L_1) and negative taper was present distally. (below) Three tapers were present in patients with aneurysms: flaring distal to renals, narrowing proximal to the throat and finally, flaring to the apex. All cross-sections were found to be circular from CT. (Diagram not to scale)

Table 5.1 Infrarenal aortic diameter measured form aortograms of normal patients.

		Diameter change (%)			Diameter taper	
Patient	Age	Pre-throat	Pre-apical	L1/L2	Pre-throat	Pre-apical
N1	49	-21.7	42.6	3.4	0.06	-0.66
N2	61	-23.2	90.6	4.3	0.15	-0.69
N3	62	-2.0	24.5	2.6	0.01	-0.36
N4	64	-22.6	26.8	3.7	0.08	-0.55
N5	69	-35.7	66.7	2.8	0.10	-0.97
N6	69	-1.6	34.6	2.6	0.03	-0.63
N7	70	-22.2	74.1	3.0	0.06	-0.72
N8	70	-3.7	24.2	1.8	0.06	-0.46
Average [±SEM]	64.3 [2.5]	-16.6 [4.4]	47.4 [9.0]	3.0 [0.3]	0.07 [0.02]	-0.63 [0.06]

L1/L2 represents the ratio of pre-throat length to pre-apical length, respectively. Taper was calculated as thechange in aortic diameter divided by the linear distance over which the change occurred. Negative taper corresponded to an expansion.

Table 5.2 Data obtained from aortograms of patients with an aneurysm.

Patient	Patient age (yrs)	Diameter change (%)			Diameter taper		
		Pre-An	Post-An	Pre-Ap	Pre-An	Post-An	Pre-Ap
An1	51	40.7	-39.5	84.8	-0.37	0.33	-0.65
An2	62	10.3	-33.3	38.0	-0.09	0.15	-0.19
An3	63	68.5	-43.9	35.2	-0.57	0.37	-0.62
An4	66	105.0	-44.6	48.4	-1.66	0.54	-0.75
An5	68	163.0	-69.6	25.0	-0.28	0.37	-0.49
An6	74	13.4	-72.6	15.8	-0.21	0.36	-0.95
An7	78	26.4	-49.5	76.1	-0.38	0.41	-0.70
An8	79	257.8	-21.6	15.0	-1.02	0.87	-0.40
An9	80	110.0	-44.6	48.4	-0.98	0.54	-0.35
Average [±SEM]	69 [3.4]	88.3 [27.2]	-46.6 [5.4]	43.0 [8.2]	-0.62 [0.17]	0.44 [0.07]	-0.57 [0.08]

Patients with abdominal aneurysms had three regions of linear diameter change ie. taper: Pre-An (aneurysm) Post-An, and Pre-Ap (apical). Taper in each of these regions was found to be significantly different from zero.

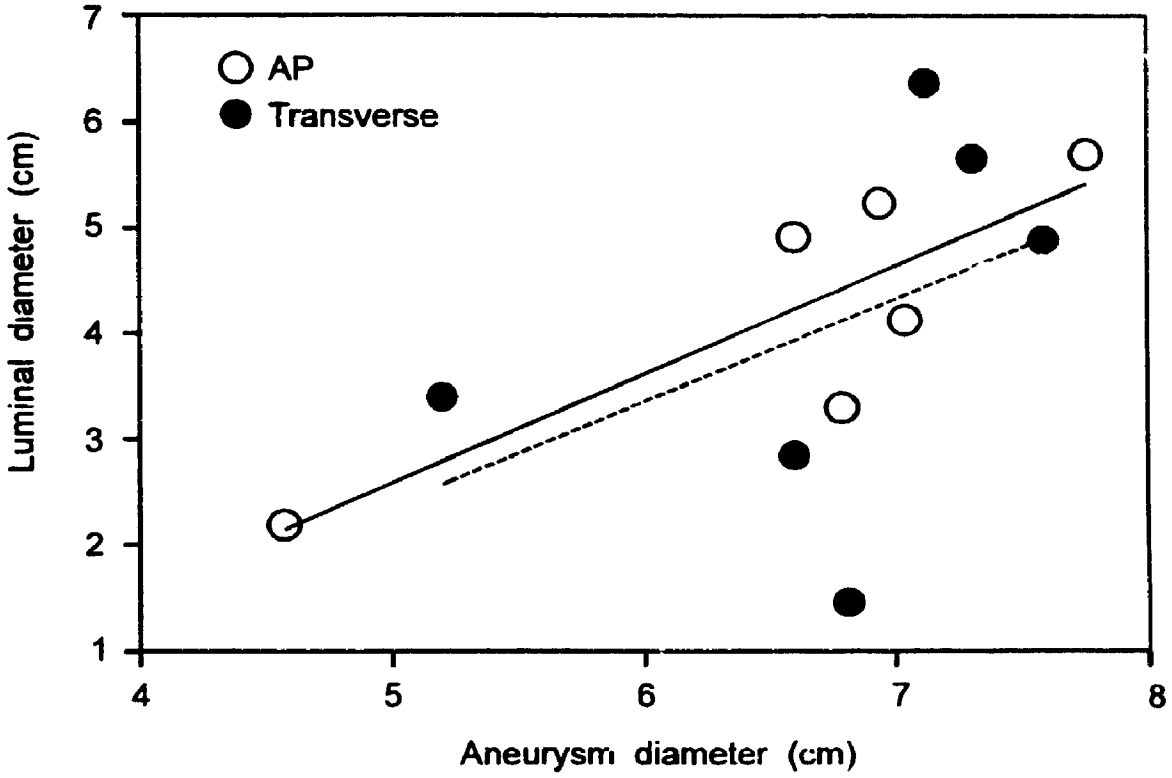

Figure 5.4 Luminal diameter tended to increase as the aneurysm diameter increased in the antero-posterior direction (solid line, $r = 0.84$ $p<0.05$). In the lateral direction, lumen diameter did not increase as the aneurysm diameter increased (dashed line).

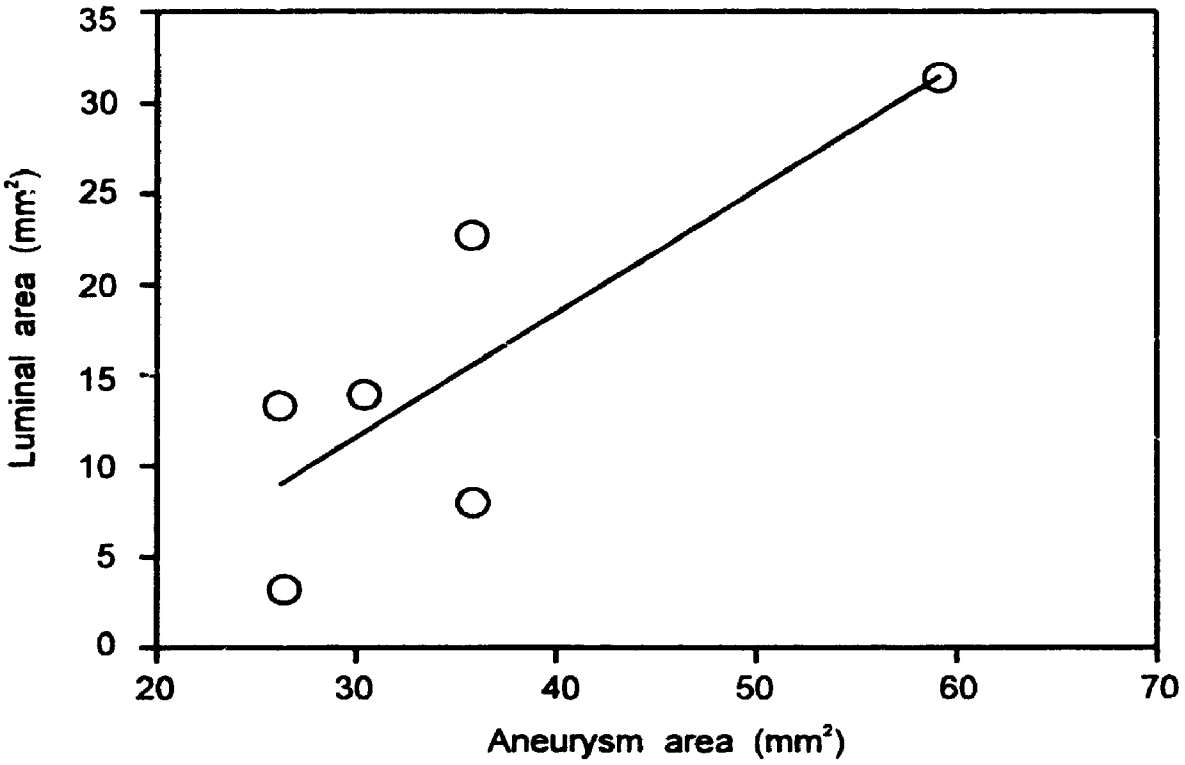

Figure 5.5 Luminal cross-sectional area tended to increase as the area of the aneurysm increased ($r=0.84$, $P<0.05$). Aneurysm area was defined as the area enclosed by the artery wall and included thrombus while luminal area represented the region available for blood flow.

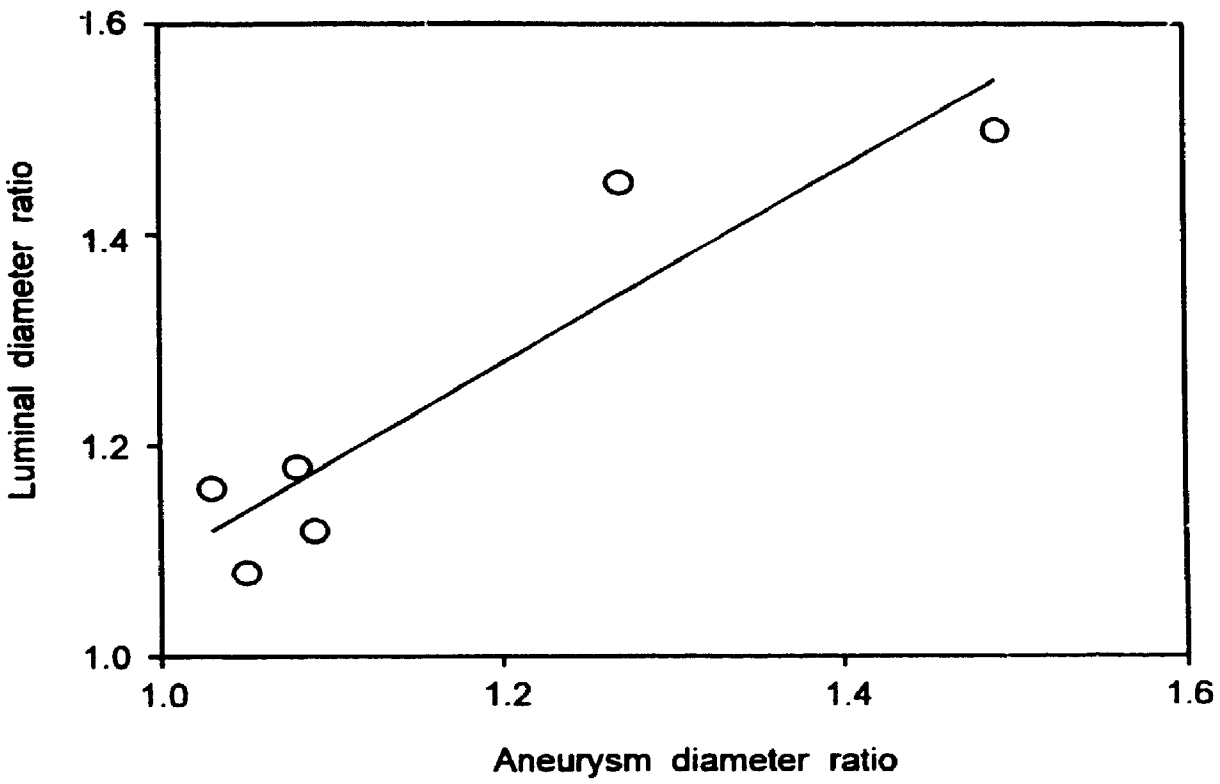

Figure 5.6 The luminal diameter tended to increase as the aneurysm diameter increased ($r=0.93$, $p<0.05$). Diameter ratio was calculated as the ratio of the length of the long axis to the length of the short axis.

Table 5.3 Analysis of luminal diameter ratio using CT.

Normals			Aneurysms		
Patient	Age	Diameter ratio	Patient	Age	Diameter ratio
CT1	26	1.06	CTA1	55	1.20
CT2	37	1.02	CTA2	61	1.12
CT3	48	1.03	CTA3	62	1.02
CT4	48	1.04	CTA4	64	1.11
CT5	49	1.02	CTA5	70	1.01
CT6	51	1.00	CTA6	71	1.27
CT7	56	1.02	CTA7	71	1.24
CT8	62	1.04	CTA8	79	1.03
CT9	63	1.00	CTA9	79	1.12
CT10	74	1.02	Average [±SEM]	68.0 [2.7]	1.13 [0.03]
CT11	75	1.04			
CT12	82	1.00			
CT13	83	1.01			
CT14	84	1.02			
Average [±SEM]	59.9 [1.3]	1.01 [0.01]			

Summary of luminal diameter ratios obtained from both normal patients and patients with abdominal aneurysms. Diameter ratio was calculated from CT images using the ratio of the long axis to short axis. No significant difference was found between the patients with and without aneurysms.

5.3.3 CT analysis of ellipticity of the lumens in normals and patients with aneurysms.

The mean ratio of long to short axis of the lumen from both normals and patients with aneurysms are shown in Table 5.3. A value of 1.0 corresponds to a circular cross-section. The mean value for the normal patients was 1.01 (±0.01 S.E.M.) and was 1.13 (±0.03 S.E.M.) for patients with abdominal aneurysms. There was no significant difference between the two groups ($P>0.05$). As a result, I concluded that the lumen was circular in cross-section for both groups from just below the renal arteries to the throat.

5.4. Discussion

Since aneurysm size is an important factor in rupture (Reilly and Tilson, 1989), it is important to determine which imaging modality gives the best resolution of the size of the aneurysm (Todd et al., 1989). This is probably the most important parameter for screening, but could not be adequately assessed with either of these radiological methods. Ultrasound, or CT with smaller slice intervals, would be more satisfactory (Vowden et al., 1989).

Most large aneurysms contain thrombus (Figure 5.1) as shown clearly in CT images obtained with contrast injection. In Figure 5.1a, which is near the origin of the aneurysm, the contrast fills most of the lumen. By comparison, in Figure 5.1d, only the centre of the lumen contains contrast and the rest is thrombosed. In this case, the lumen is near the centre of the aneurysm.

The aneurysm, which has a flared region from its origin to the aneurysm apex, and a tapered region from the aneurysm apex to its distal boundary is a good example of the effects of these luminal area changes on flow. The velocity will decrease as in the flared region and increase past it. In the flared region, a

separation zone will develop, the flow will be stagnant, and so thrombus develops. This is most common in large aneurysms and the thrombus often continues to develop until the area of the lumen is comparable to that seen in the normal aorta.

Since muscle is destroyed in the aneuyrsm wall (He, 1992), the wall itself cannot remodel as occurs in the normal aorta (Zarins et al., 1987), but instead, the lumen remodels with thrombus.

In CT scans, the major limitation is that the cuts are 5mm thick (1cm with older machines), resulting in an image that is an average over that longitudinal distance. This makes the resolution considerably less if taper or curvature is present. CT, however, has two great advantages. First, it shows both the wall of the aneurysm and also the lumen of the aorta (when contrast is used). Second, it allows measurements of circularity or ellipticity. Since the aneurysm bulges significantly, and the lumen is often fairly normal, CT allows crude measurements of relative changes of lumen and aneurysm size.

Glagov et al. (1992) have suggested that the walls of vessels remodel to maintain a shear stress of 1.5 N/m^2. Most authors accept that endothelial cells are sensitive to shear stress and secrete factors such as endothelial-derived growth factor or relaxing factor (Langille and O'Donnell, 1986). It seems unlikely that this plays a role in remodelling the lumen of the aneurysms. The aneurysms are often in regions that are heavily involved with atherosclerosis, and the endothelium may be damaged. In addition, the muscle cells are usually destroyed. Instead, the remodelling occurs with the development of thrombus. Platelets are known to adhere to regions with damaged endothelium (Goldsmith, 1974). This stimulates the release of a variety of clotting factors and the thrombus begins to form. In addition, vortex formation occurs in separation zones (regions with an increase in cross-sectional area), and platelets have been shown to clump in these regions. I speculate that the thrombus is laid down to eliminate separation zones, and so

would be totally dependent on the flow patterns.

The changes in wall shear stress are harder to assess (Stringfellow et al., 1987). The Law of Laplace has been used to calculate the tension from the product of pressure and radius (Roach and Burton, 1957), but assumes that the wall is thin, the radius of curvature is uniform and the wall is isotropic. While this may be applicable before the thrombus develops, it is not true once thrombus is present. As mentioned above, the elastic properties of the thrombus are unknown.

What makes most aneurysms stop at the throat? Based on flow arguments, because the region from the throat to the flow divider flares, and becomes more elliptical (Chapter 4), there should be separation zones that give rise to thrombus. However, because this region is elliptical, the bending energy at the lateral angles will be much higher than that of the anterior and posterior walls. This could prevent the formation of a fusiform aneurysm as the wall would not stretch uniformly.

In many cases, as shown in Figure 5.1, the lumen is the centre of the aneurysm, while in others it is quite skewed. This could be due to local factors such as atherosclerotic plaques or ulcers, or could be due to tortuosity; both are known to alter blood flow patterns. Since I cannot measure tortuosity from CT's (due to section thickness) and cannot measure the aneurysm wall from aortograms (since only the lumen is visible), I am unable to answer this question.

There is an emerging theme that the area ratio of the iliacs to the aorta plays an important role in the genesis of atherosclerosis (Gosling et al., 1971; Lallemand et al., 1972; Lallemand et al., 1973; Newman and Bowden, 1973; Bargeron et al., 1986; Friedman, 1989). Area ratios were measured at only one location in each branch. Obviously, the extent of the taper that I have reported here makes single measurements of aortic (and probably iliac) diameter unwise.

In summary, this study has shown that:

(1) large tapers occur in the infrarenal aorta in both normal patients and in patients with aneurysms,

(2) the lumen was circular in cross-section from the renals to the throat in both patient groups, and,

(3) luminal area and the aneurysm area were linearly related and both circular in cross-section in the region of maximum aneurysm diameter.

The implications of these results are:

(1) measurements of single diameters as used now clinically for screening patients for aneurysms are not reliable due to large changes in aortic diameter. Meaurements of taper are more reliable.

(2) diameter and area tapers are compable in the aneurysm region due to circular symmetry. Thus, 2D aortography can be used reliably to measure aneurysm size. The asymmetrical region between the aneurysm throat and the flow divider requires 3D geometry to study geometry due to the asymmetry of cross-sections.

(3) the lumen of aortic aneurysms remodels with thrombus in order to restore normal luminal geometry. As a result, average flow velocity through an abdominal aortic aneurysm may be similar to flow through a normal abdominal aorta.

(4) average flow through the normal infrarenal aorta accelerates between the renal arteries and the throat and then decelerates from the throat to the flow divider. Flow in an aneurysmal aorta without thrombus would be considerably different from that in the normal aorta. Flow would enter the large expansion and would decelerate to the aneurysm apex. Distal to the aneurysm apex,

flow would accelerate through the tapered reion to the throat and then decelerate from the throat to the flow divider.

Chapter 6

Conclusions

In this thesis, I have presented a detailed analysis of how area taper varies in two Y-bifurcations: the porcine renal (a Y-junction of the muscular type) and the human aorto-iliac bifurcation (a Y-junction of the elastic type). I have also reanalysed data from Macfarlane (1985) on human cerebral bifurcations (muscular) to determine if the geometry of cerebral arteries which develop aneurysms at the apex of bifurcations are different from the porcine renal or human aorto-iliac bifurcation.

The major conclusions of this study are:

1) All of the arteries studied have significant taper both proximal and distal to the flow divider. This means that previous flow models which have assumed the arteries were straight except immediately adjacent to the flow divider will have incorrect conclusions.

2) The presence of taper makes conclusions based on area ratios difficult to evaluate. Most authors have used area ratios. Some have specified that they are measured one parent diameter on either side of the flow divider (as I have done), but others do not state where the measurements are made. I believe that taper is a more reliable parameter.

3) Area taper, a concept which I have introduced and is defined as the change in luminal cross-sectional area per unit length of artery, will lead to acceleration (if artery tapers) or deceleration (if artery flares) of blood flow. Large tapers may lead

to separation zones which could decrease the associated deceleration and would produce ever lower shear stresses at the wall.

4) Diameter taper, the term used by others and defined as the change in diameter per unit length of artery, is related to area taper if the lumen is circular in cross-section, but not if it is elliptical. Near the bifurcation, the lateral diameter increases to form the branches, and the antero-posterior diameter decreases to form the flow divider. In this region, which in the aorta is about one aortic diameter long, diameter taper and area taper are unrelated. Here, while there may be an average deceleration of flow, the velocities near the anterior and posterior walls may increase while those near the lateral wall may decrease. The junctions of these could have very large differences in shear stress over quite short distances. This will have to be tested either theoretically or experimentally in the future. Three dimensional ultrasound is being developed currently and may be able to do this within the next three years although it cannot do so at present.

5) The luminal geometry and the wall thickness of the human aorto-iliac bifurcation changed from day 1 to age 76 yrs. At birth, the abdominal aorta is thin posteriorly while the rest of the aorta is uniformly thick along its length. By age 19, the lateral regions are thicker than the antero-posterior region but the total wall thickness decreases along the aorta and proximal to the aorto-iliac bifurcation. Although it has been well documented that atherosclerosis and hypertension increase wall thickness, the changes that I have reported for the very young arteries are likely due to the dramatic changes in blood flow that occur at birth. Zarins and Glagov (1987) have suggested that wall thickness is related to tensile stress. My data suggests that there must be large variations in tensile stress around the aorta at any cross-section along its length. Laplace's law which relates tensile stress to

the product of luminal pressure and radius, has ben used widely to calculate circumferential tension in the aorta but it assumes the wall is isotropic. My data implies that Laplace's law should not be used to calculate tension in the lower abdominal aorta.

6) Aneurysms are known to develop at the apex of bifurcations of human cerebral bifurcations, but not at other bifurcations. There is still debate whether they are due to hemodynamic factors as suggested by Ferguson (1972), or to structural differences in the wall in this region (Stehbens, 1975). Elastin is absent from cerebral aneurysms, and presumably they develop when the elastin is destroyed. My data shows no significant difference in luminal geometry in human cerebral arteries and porcine renal arteries. This suggests that hemodynamic factors are unlikely to play a major role in the develop of aneurysms. Variations in arterial wall thickness are known to occur. More detailed studies of this, and of the variations in wall thickness in the bifurcation region of cerebral arteries are required.

7) Abdominal aortic aneurysms occur preferentially between the renal arteries and the throat. I have shown that this region tapers in contrast to the flaring seen in other 'straight' positions of arteries. Thus it seems likely that the shear stress acting on the wall is quite different here than in other arteries. This may explain why atherosclerosis occurs diffusely in this region, but primarily at bifurcations in other parts of the arterial tree.

8) The region of the infrarenal aorta from the throat to the flow divider is a distinct region in the abdominal aorta and was not seen in either the renal or cerebral bifurcations. Here the aorta tapers dramatically, so that in contrast to the muscular bifurcation where flow decelerates towards the flow divider, here it accelerates.

Nobody else has described this dramatic difference, nor mapped the difference in the distribution of atherosclerotic lesions in this zone. In most cases, aneurysms do not appear to extend into this zone.

9) The human infrarenal aorta and aorto-iliac bifurcation change with age, but I found no significant difference in porcine renal arterial bifurcations from young (6-14 wk) and old pigs (>1 yr). Pigs reach maturity at approximately 5 years (Dr. S Fussel, personal communication) while humans reach maturity at 13-15 years. This suggests that the age of the renal arteries studied would be equivalent to approximately a 5 month and a 5 year old human, respectively. In view of the fact that the most dramatic changes in the aorta were in infants < 1 year of age, studies should probably be done on renal arterial bifurcations from weanling pigs.

Chapter 7

Future work and the application of area taper to flow studies

7.1 Taper and atherosclerosis

Taper was defined as the ratio of luminal cross-sectional area (mm^2) to the unit length of artery (mm) thus having units of mm. Alternatively, taper can be described by the angle subtended between the axis of symmetry of the branch and the artery wall. This is shown in the top panel of Figure 6.3 where 'θ' denotes the angle between the artery wall and the axis of symmetry of the branch. The effect of taper on flow patterns has been studied previously in glass tubes having taper angles between 1 and 2° (Buss, 1980). Fox and Hugh (1966) showed mathematically, that flow entering an expansion forms a separation zone, and, that the length and flow velocities within this zone were related to the Reynolds' number. The formation of a separation zone has important implications in the development of atherosclerotic lesions since this increases the duration of exposure of circulating atherogenic agents to the intimal surface. Separation zones also provide favourable conditions for transendothelial diffusion or intimal entrapment of atherogenic particles (Glagov et al., 1988).

7.1.1 Formation of a separation zone in an expansion

When flow occurs over a surface, the layer closest to the wall has zero velocity relative to the surface due to frictional stresses exerted upon the fluid by the surface. This is the 'no-slip' condition.

An increase in the cross-sectional area available for flow reduces the average flow velocity in the direction of blood flow in order to maintain the continuity of flow. Since the energy of the system is conserved, energy lost due to fluid deceleration is converted to pressure energy while some of the energy is lost to friction. Due to

the momentum of the moving fluid, the fluid is able to pass from a region of low pressure into a region of higher pressure, i.e. against a positive pressure gradient. As a result, flow near the intima, having low momentum, can be brought to rest rapidly due to the increase in pressure. As flow proceeds further into the expansion, the average flow velocity continues to decrease and the region of stasis or stopped flow increases. Without the positive pressure gradient, flow in the separation zone would have zero velocity. A large, positive, pressure gradient can cause reverse flow patterns in the separation zone. This is shown schematically in figure 7.1.

The velocity of the fluid in the separation zone has been shown experimentally to be related to the Reynolds' number. Reynolds' number is the ratio of inertial forces to the viscous forces of the fluid, or mathematically,

$$Re = \rho v d/\eta , \qquad (1)$$

where ρ is fluid density, v, average flow velocity, d is tube diameter and η represents the viscosity of the fluid. When the frictional forces of the fluid are greater than the inertial forces, then the reverse velocity in the separation zone will be low; conversely, when the inertial forces exceed frictional forces, then flow velocity in the separation zone will be high.

7.1.2 Formation of separation zones in arterial Y-bifurcations

Previous studies have shown that separation zones can form where there is a net increase in cross-sectional area. We can apply this knowledge to the bifurcations examined in this thesis and speculate about the flow patterns produced proximal to the flow divider of these branches. Figure 7.2 illustrates three models that have taper proximal to the flow divider of an arterial bifurcation. In order to further simplify these models, I will make the following assumptions:

1) the bifurcation is circular in cross-section (this is true away from the flow divider, chapter 4), and,

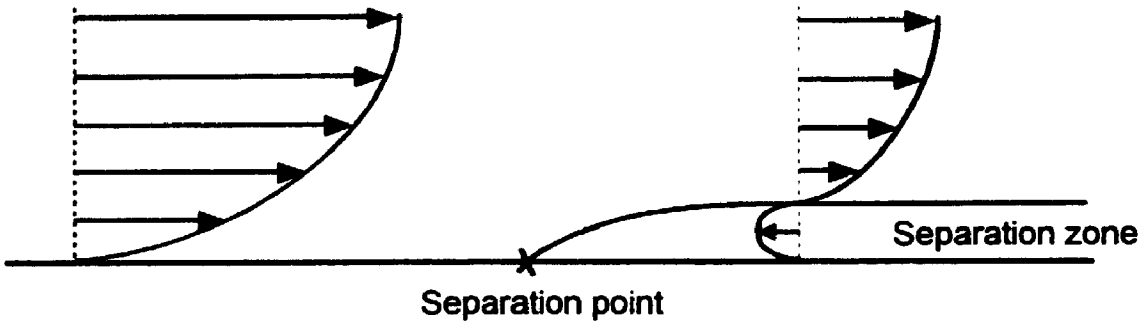

Figure 7.1 Schematic diagram showing the steps involved in producing a separation zone. Separation zones are formed in an expansion since the fluid decelerates to maintain continuity of flow. As flow decelerates, some of the energy is converted to pressure. This produces a positive pressure gradient along the tube which if great enough, can produce a separation zone with retrograde flow.

2) flow entering the bifurcation is non-pulsatile and laminar (fully-developed)

Bifurcation A: flow enters the bifurcation and forms a separation zone along lateral walls of the bifurcation. The Reynolds' number and the magnitude of the expansion will determine whether or not the zone forms, as well as the location of the separation and re-attachment points along the wall. At the apex, the flow field is divided evenly into each of the daughter branches. The expansion zone decelerates flow, proximal to the flow divider. The daughter branches have a constant diameter and flow through this region would likely re-establish a fully-developed, parabolic profile faster than in a bifurcation without the proximal expansion. Flow disturbances produced at the apex will be greatly reduced as a result of flow deceleration proximally.

Bifurcation B (modelled after the porcine renal arterial bifurcation): as in 'Bifurcation A', the formation of a separation zone will be determined by both the Reynolds' number and by the magnitude of the expansion. In the daughter branches, flow enters the tapered region causing the average velocity to increase and the pressure to decrease. The effect of increased flow velocity through the region of reduced cross-sectional area should increase flow stability. As a result, the effect of the bifurcation apex on flow is minimized greatly by the expansion zone proximally, and by the taper distally.

Bifurcation C (modelled after the human aorto-iliac bifurcation): in this model, the expansion and tapered regions have been moved proximal to the apex of the bifurcation, and a second expansion zone added distal to the apex. The flow patterns produced in the bulge proximal to the apex will likely be similar to those described in 'Bifurcation B'. As flow approaches the apex, it will be stabilized due

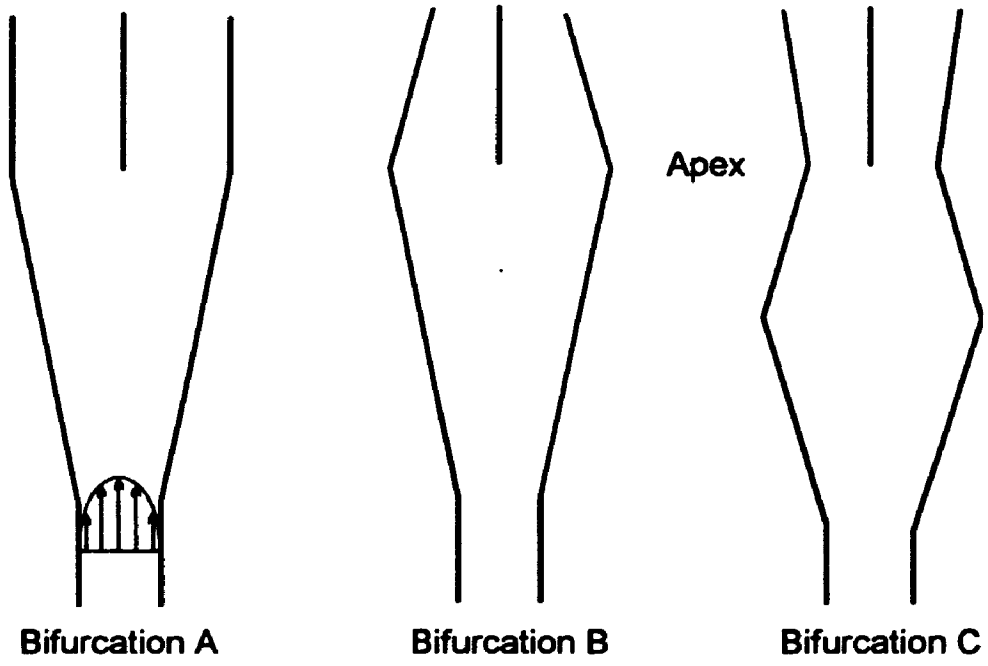

Figure 7.2 Three models of an arterial bifurcation. In each of these models, the effect of branch angle has been ignored. (A) This bifurcation has a linear expansion in cross-sectional area proximal to the flow divider; distal to the apex, the summed daughter area is constant. (B) This bifurcation represents the geometry found in both human cerebral bifurcations and porcine renal bifurcations. There is a large expansion region proximal to the apex, the area is maximum at the flow divider, followed by taper in the daughter branches. (C) This is the geometry observed in the human aorto-iliac bifurcation. There is an expansion followed by a tapered region proximal to the apex. The maximum area was always proximal to the flow divider. Distal to the flow divider, luminal cross-sectional area increased. This diagram is not to scale.

to the tapered region, divides at the apex, and then decelerates again distal to the flow divider possibly forming a second separation zone in the daughter branches.

7.1.3 Finite element analysis of flow through parent trunk of Bifurcation B

Previous studies of flow patterns produced in a tapered tube (Buss, 1980; Fox and Hugh, 1966) have used taper angles of 1 to 2 degrees. In order to convert the taper in the porcine renal artery to an angle, we must assume that the parent trunk of the bifurcation is circular in cross-section. By doing so, the average taper angle in the parent trunk of the porcine renal bifurcation is 7.2°. This is an enormous taper compared to the magnitude of the tapers studied previously.

With the collaborative support of Dr. M. Nakamura from the Department of Mechanical Engineering, Akita University, Japan, we have constructed a 2-dimensional finite element model of the parent branch of the porcine renal bifurcation to study the effect of large taper angles on flow patterns. The inlet and outlet diameters used in this study were obtained from the data presented in this thesis. Flow patterns were studied using both Newtonian and Casson fluids. The Casson fluid was used to mimic the non-Newtonian properties of blood. A schematic diagram of the model is shown in figure 7.3. The preliminary results of this study (figure 7.3) suggest that separation zones can form with Newtonian fluids at low Reynolds' numbers (i.e. 70) if the taper angle is sufficiently large while higher Reynolds' numbers were required to create a separation zone with the Casson fluid. The results from these preliminary studies suggest that separation zones are created distally initially, and then propagate retrograde. Further studies will be required to examine the effect of the flow divider on the location of the separation zones and to correlate the location of thee separation zones with the localization of atherosclerotic lesions.

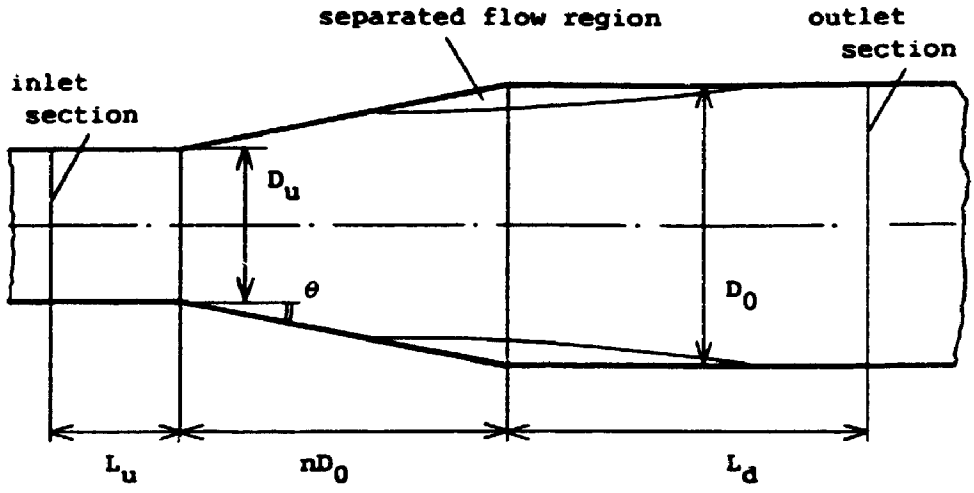

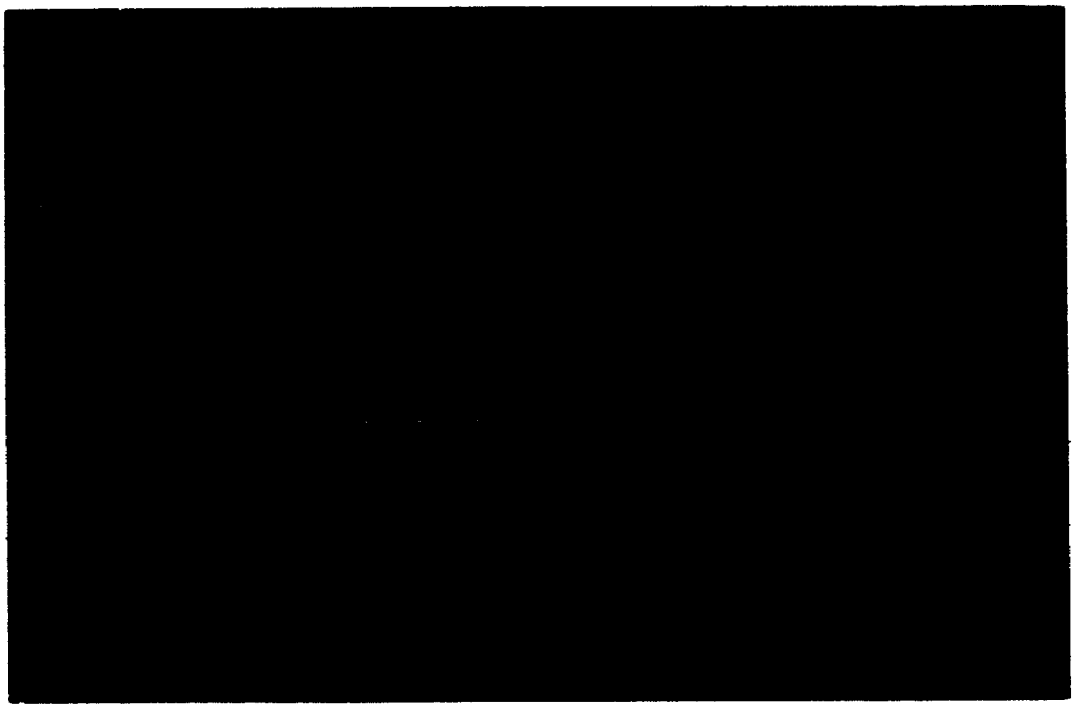

Figure 7.3 (Top) Schematic diagram of the axisymmetric tube studied using finite element analysis. (Bottom) Results of the finite element model used to study flow patterns in an expansion. The blue arrows represent forward flow while red arrows indicate the regions of flow reversal. The magnitude of the flow velocity is proportional to the length of the arrow-head (see scale). The terms I/O and L in the bottom panel correspond to D_u/D_0 and nD_0 in the top panel, respectively. These figures were reproduced with Dr. Nakamura's permission.

7.2 *In vivo* geometrical analysis of the human infrarenal aorta.

The infrarenal aorta is predisposed to the development of both severe atherosclerotic lesion involvement as well as to aneurysm formation. Human infrarenal geometry was examined from aortograms with contrast injection while the shape of the aorta was examined from computed tomographic (CT) images. CT showed that the aorta was circular in cross-section in both the normal infrarenal aorta as well as in an infrarenal aortic aneurysm while aortograms revealed two large, linear changes in luminal diameter in normal patients and three diameter tapers in patients with aortic aneurysms.

The factors associated with aneurysm development remain unclear. He (1992) compared the mechanical properties and the composition of a human aortic aneurysm to the normal aorta. He showed that the wall of an aneurysm consists of collagen and ground substance while elastin and smooth muscle cells were noticeably absent. The lack of elastin in the aneurysm wall could explain why aneurysms were very stiff compared to the normal aorta. The normal aorta becomes stiffer with increasing age due to the fragmentation of medial elastin and to an increase in collagen to elastin ratio (Robert et al., 1987). Robert has also suggested that the fragmentation of medial elastin could be due to an increase in circulating proteases with age. However, this also remains to be proven. The effect of age on the aortic wall mirrors the process of aneurysm formation since both age and aneurysms render the aorta very stiff and also reduces greatly the elastin concentration in the tunica media. This leads to the question: are aneurysms simply the result of an accelerated aging process? This question is likely impossible to answer due to all of the factors competing simultaneously.

7.3 Future Work

The results of the experiments discussed in this thesis have raised a lot of questions. Some of these questions are being addressed currently while others remain unchallenged.

7.3.1 Wall thickness composition

Maps of circumferential wall thicknesses in the parent of the human aorto-iliac bifurcation revealed that the artery wall was thickest laterally and thinnest in the antero-posterior direction in all but two of the youngest patients examined. In the very youngest (1 day), the parent trunk was thinnest posteriorly, or adjacent to the spine and uniform in thickness everywhere else while the aorta was thickest laterally and thinnest in both the anterior and posterior directions in the 41 year old. These circumferential variations are maintained along the entire length of the parent. As a result, there must be a difference in the composition, and hence, mechanical properties in each of these quadrants. This leads to two studies: first, to examine histologically, changes in wall composition in each of these quadrants and, second, to examine the mechanical properties of each these quadrants. To my knowledge, neither of these studies has been undertaken previously.

7.3.2 *In vivo* ultrasound imaging of infrarenal aorta

The geometrical studies that I have reported in Chapters 2, 3 and 4 were performed on excised tissue obtained at autopsy and pressure fixed at mean arterial pressure. The *in vivo* measurements of the infrarenal aorta reported in Chapter 5 were obtained from aortograms and CT images that were averaged over several cardiac cycles. Real-time dimension changes of the infrarenal aorta can be measured from two orthogonal views of the human infrarenal aorta over the cardiac cycle with a clinical ultrasound machine.

In collaboration with Drs. Roach and Rankin and the Ultrasound Department at University Hospital, London, Ontario, I have recently started measuring changes in infrarenal aortic diameter between systole and diastole. The results of this study may provide new information concerning the geometrical and mechanical properties of the infrarenal aorta *in vivo*.

7.3.3 Histological analysis of the infrarenal aorta

The propagation of infrarenal aneurysms seems to be halted at the throat in all of the patients that I have examined. The throat was defined by Bargeron et al. (1986) as the narrowest part of the aorta but the function of the throat remains unclear. Since aneurysms are thought to be formed by degrading elastin and smooth muscle, the composition or the organization of the components in the throat region may serve as a barrier to the propagation of aneurysms into the iliac vessels. A histological analysis of the throat may provide us with clues concerning why there is a narrowing as well as how this narrowing alters aneurysm development. This remains to be studied.

References

Amparo, E.G., Hodick, W.K., Hricak, H., Sollito, R., Justich, E., Filly, R.A. and Higgins, C.B. (1985). Comparison of magnetic resonance imaging and ultrasonography in the evaluation of abdominal aortic aneurysms. Radiology 154: 451-456.

Avolio, A. (1992) Ageing and wave reflection. J Hypertens Suppl 10: S83-86.

Bandyk, D.F. (1989). Pre-operative imaging of aortic aneurysms: Conventional and digital subtraction aortography, computed tomography scanning, and magnetic resonance imaging. Surg Clin N Am 69: 721-735.

Bargeron, C.B., Hutchins, G.M., Moore, W., Deters, O.J., Mark, F.F. and Friedman, M.H. (1986). Distribution of the geometrical parameters of human aortic bifurcations. Arteriosclerosis 6: 109-113.

Brech, R. and Bellhouse, B.J. (1973). Flow in branching vessels. Cardiovasc Res 7: 593-600.

Burton, A.C. (1962). Phyisical principles of circulatory phenomena: the physical equilibria of the heart and blood vessels. In, Handbook of Physiology, Section 2: Circulation. Editors, Hamilton, W.F. and Dow, P. Waverly Press, Baltimore. pp. 85-106.

Buss, G.Y. (1980). Transition to turbulence in a model of the human superficial femoral artery. In, Blood flow: theory and practice. Editors, Taylor, D.E.M. and Stevens, A.L. Academic Press, Toronto. pp. 7-37.

Caro, C.G., Fitz-Gerald, J.M. and Schroter, R.C. (1971). Atheroma and arterial wall shear: Observation, correlation and proposal of a shear dependent mass transfer mechanism for atherosclerosis. Proc R Soc Lond [Biol] 117: 109-159.

Caruso, H.A. and Ferreri, J.C. (1975). Oscillatory flow in a Y-shaped bifurcation. Acta physiol latinoam 25: 271-278.

Castleden, W.M., Mercer, J.C. and Members of the West Australian Vascular Service. (1985). Abdominal aortic aneurysms in Western Australia: descriptive epidemiology and patterns of rupture. Br J Surg 72: 109-112.

Cole, C.E. (1989). Highlights of an international workshop on abdominal aortic aneurysms. Can Med Assoc J 141: 393-395.

Ferguson, G.G. (1972). Physical factors in the initiation, growth and rupture of human intracranial saccular aneurysms. J Neurosurg 37: 666-677.

Feuerstein, I.A., ElMasry, O.A. and Round, G.F. (1976). Arterial bifurcation flows-effects of flow rate and area ratio. Can J Physiol Pharmacol 54: 795-808.

Fowkes, F.G.R., Macintyre, C.C.A. and Ruckley, C.V. (1989). Increasing incidence of aortic aneurysms in England and Wales. Brit Med J 289: 33-35.

Fox, J.A. and Hugh, A.E. (1966). Localization of atheroma: A theory based on

boundary layer separation. Brit Heart J 28: 388-399.

Friedman, M.H. (1989). A biologically plausible model of thickening of arterial intima under shear. Arteriosclerosis 9: 511-522.

Friedman, M.H., Bargeron, C.B., Hutchins, G.M. and Mark, F.F. (1980). Hemodynamic measurements in human arterial casts and their correlation with histology and luminal area. J Biomech Eng 102: 247-251.

Friedman, M.H. and Ehrlich, L.W. (1984). Numerical simulation of aortic bifurcation flows: The effect of flow divider curvature. J Biomech 17: 881-888.

Friedman, M.H., Hutchins, G.M., Bargeron, C.B., Deters, O.J. and Mark, FF. (1981). Correlation between intimal thickness and fluid shear in human arteries. Atherosclerosis 39: 425-436.

Fry, D.L. (1968) Acute vascular endothelial changes associated with increased blood velocity gradients. Circ Res 22: 165-197.

Glagov, S., Zarins, C.K., Giddens, D.P. and Ku, D.N. (1988). Hemodynamics and atherosclerosis: Insights and perspectives gained from studies on human arteries. Arch Path Lab Med 112: 1018-1031.

Glagov, S., Vito, R., Giddens, D.P. and Zarins, C.K. (1992). Micro-architecture and composition of artery walls: relationship to location, diameter and the distribution of mechanical stress. J Hypertens Suppl 10: S101-104.

Goldsmith, H.L. (1974). Blood flow and thrombosis. Throb diathes haemorrh 32: 35-48.

Gosling, R.G., Newman, D.L., Bowden, N.L.R. and Twinn, K.W. (1971). The area ratio of normal aortic junctions: Aortic configuration and pulse-wave reflection. Br J Radiol 44: 850-853.

Greenwald, S.E., Carter, A.C. and Berry, C.L. (1990). Effect of age on the in vitro reflection coefficient of the aorto-iliac bifurcation in humans. Circulation 82: 114-123.

Hassler, O. (1961). Morphological studies on the large cerebral arteries with reference to the aetiology of subarachnoid haemorrhage. Acta psychiat neurol scand 36: suppl. 154, pp 5-67.

He, C.M. The composition and mechanical properties of abdominal aortic aneurysms. M.Sc. Thesis. University of Western Ontario. London, Ontario, 1992.

Hoogendam, I.J., VanRinsum, A.C. and Olyslager, J. (1984). The diameter of the distal abdominal aorta and the aetiology of local atheroma. J Cardiovasc Surg 25: 408-413.

Houle, S. and Roach, M.R. (1981). Flow studies in a rigid model of an aorto-renal junction: A case for high shear as a cause of the localization of sudanophilic lesions in rabbits. Atherosclerosis 40: 231-244.

Kandarpa, K. and Davids, N. (1976). Analysis of the fluid dynamic effects on

atherosclerosis at branching sites. J Biomech 9: 734-741.

Karino, T. and Goldsmith, H.L. (1985). Particle flow behaviour in models of branching vessels: II. Effects of branching angle and diameter on flow patterns. Biorheology 22: 87-104.

Kratky, R.G., Lo, D.K. and Roach, M.R. (1991). Quantitative measurement of fixation rate and dimension changes in the aldehyde/pressure-fixed canine carotid artery. Blood Vessels 28:386-395.

Ku, D.N., Giddens, D.P., Zarins, C.K. and Glagov S. (1985). Pulsatile flow and atherosclerosis in the human carotid bifurcation: Positive correlation between plaque location and low and oscillating shear stress. Arteriosclerosis 5: 293-302.

Lallemand, R.C., Brown, K.G.E. and Boulter, P.S. (1972). Vessel dimensions in premature atheromatous disease of the aortic birurcation. Brit Med J 2: 255-257.

Lallemand, R.C., Gosling, R.G. and Newman, D.L. (1973). Role of the bifurcation in atheromatosis of the abdominal aorta. Surg Gyn Obstet 137: 987-990.

Langille, B.L. and O'Donnell, F. (1986). Reductions in artaterial diameter produced by chronic decreases in blood flow are endothelium dependent. Science 231: 405-407.

Lee, Y-T.N., Keitzer. W.F., Watson, F.R. and Liu, H. (1982). Vascular geometry at the abdominal aortic bifurcation. JAMWA 37: 77-81.

Ludin, H., Juabin, E.J., Kaufmann, H.J. and vonPein, W. (1971). Significance of alterations in main renal artery calibre and configuration. Acta Radiol 12: 803-832.

Lynn, N.S., Fox, V.G. and Ross, L.W. (1972). Computation of fluid-dynamical contributions to atherosclerosis at bifurcations. Biorheology 9: 61-66.

Macfarlane, T.W.R. (1985). A computer-based quantitative image analysis of the geometry of the human cerebral arterial bifurcations. Ph.D. Thesis, University of Western Ontario, London, Ontario, pp 62-94.

Macfarlane, T.W.R., Canham, P.B., and Roach, M.R. (1983a). Shape changes at the apex of isolated human cerebral bifurcations with changes in transmural pressure. Stroke 14: 70-76.

Macfarlane, T.W.R., Petrowski, S., Rigutto, L. and Roach, M.R. (1983b). Computer based video analysis of cerebral arterial geometry using the natural fluorescence of the arterial wall and contrast enhancement techniques. Blood Vessels 20: 161-171.

MacLean, N.F., Kratky, R.G., Macfarlane, T.W.R., and Roach, M.R. (1992) Taper: an important feature of Y-bifurcations in porcine renal arteries and human cerebral arteries. J Biomech 25: 1047-1052.

Malcolm, A.D. and Roach, M.R. (1979). Flow disturbances at the apex and lateral angles of a variety of bifurcation models and their role in development and manifestations of arterial disease. Stroke 10: 335-343.

Mark, F.F., Bargeron, C.B., Deters, O.J. and Friedman, M.H. (1989). Variations in geometry and shear rate distribution in casts of human aortic bifurcations. J Biomech 22: 577-582.

McClave, J.T. and Dietrich, F.H. (1986). A first course in statistics. San Francisco: Dellen , p296.

Murray, C.D. (1926a). The physiological principle of minimum work. I. The vascular system and the cost of blood volume. Proc Nat Acad Sci (USA). 12: 207-244.

Murray, C.D. (1926b). The physiological principle of minimum work applied to the angle of branching of arteries. J Gen Physiol 9: 835-841.

Musto, R. and Roach, M.R. (1980). Flow in glass models of aortic aneurysms. Can J Surg 23: 452-455.

Newman, D.L. and Bowden, N.L.R. (1973). Effect of reflection from an unmatched junction on the abdominal aortic impedance. Cardiovasc Res 7: 827-833.

Perktold, K. (1987). On the paths of fluid particles in an axisymmetrical aneurysm. J Biomech 20: 311-317.

Pond W.G. and Houpt, K.A. (1978). The Biology of the Pig. , Ithaca, N.Y.: Comstock, p31.

Rayman, R., Kratky, R.G. and Roach, M.R. (1985). Steady flow visualization in a rigid canine aortic cast. J Biomech 18: 863-875.

Reilly, J.M. and Tilson, M.D. (1989). Incidence and etiology of abdominal aortic aneurysms. Surg Clin N Amer 69: 705-711.

Roach, M.R. and Burton, A.C. (1957). The reason for the shape of the distensibility curves of arteries. Can J Biochem Physiol 35: 681-690.

Roach, M.R. and MacLean, N.F. (1993). The importance of taper proximal and distal to Y-bifurcations in arteries. Front Med Biol Engng 5: 127-133.

Robert, L., Labat-Robert, J. and Hornebeck, W. (1987). Ageing and atherosclerosis. In: Atherosclerosis Reviews, edited by A.M. Gotto Jr. and R. Paoletti. New York: Raven Press, pp. 143-170.

Smith, R.L., Blick, E.F., Coalson, J. and Stein, P.D. (1970). Thrombus production by turbulence. J Appl Physiol 32: 311-317.

Stehbens, W.E. (1974). Changes in the cross-sectional area at the arterial fork. Angiology 25: 561-575.

Stehbens, W.E. (1975). Ultrastructure of aneurysms. Arch Neurol 32: 798-807.

Stringfellow, M.M., Lawrence, P.F. and Stringfellow, S.M. (1987). The infuence of aorto-aneurysm geometry upon stress in the aneurysm wall. J Surg Res 42: 425-433.

Tabbara, M., White, R., Cavaye, D. and Kopchok, G. (1991), In vivo human

comparison of intravascular ultrasonography and angiography. J Vasc Surg 14: 496-502.

Thiriet, M., Pares, C., Saltel, E., and Hecht, F. (1992). Numerical simulation of steady flow in a model of the aortic bifurcation. J Biomech Engng 114: 40-49.

Todd, G.J., Nowygrodk, R., Benvenisty, A., Buda, J. an Reemtsma, K. (1989). The accuracy of CT scanning in the diagnosis of abdominal and thoracoabdominal aortic aneurysms. J Vasc Surg 13: 302-310.

Vowden, P., Wilkinson, D., Ausbsky, J.R. and Kester, R.C. (1989). A comparison of three imaging techniques in the assessment of abdominal aortic aneurysms. J Cardiovasc Surg 30: 891-896.

Walburn, F.J. and Stein, P.D. (1980). Flow in a symmetrically branched tube simulating the aortic bifurcation: The effects of unevenly distributed flow. Ann Biomed Engng 8: 159-173.

Witte, R.S. (1989). Statistics. Holt, Rhinehart and Winston, Inc. Toronto.

Wolinsky, H. and Glagov, S. (1964). Structural basis for the static mechanical properties of the aortic media. Circ Res 14: 400-413.

Yung, C-N, DeWitt, K.J., and Keith, T.G., Jr. (1990). Three-dimensional steady flow through a bifurcation. J Biomech Engng 112: 189-197.

Zamir, M. (1976). Optimality principles in arterial branching. J theor Biol 62: 227-251.

Zamir, M. and Phipps, S. (1987). Morphometric analysis of the distributing vessels of the kidney. Can J Physiol Pharmacol 65: 2433-2440.

Zamir, M., Wrigley, S.M. and Langille, B.L. (1983). Arterial bifurcations in the cardiovascular system of a rat. J Gen Physiol 81:325-335.

Zarins, C.K., Zatina, M.A., Giddens, D.P., Ku, D.N. and Glagov, S. (1987). Shear stress regulation of artery lumen diameter in experimental atherogenesis. J Vasc Surg 5: 413-420.

5.3.3 CT analysis of ellipticity of the lumens in normals and patients with aneurysms.

The mean ratio of long to short axis of the lumen from both normals and patients with aneurysms are shown in Table 5.3. A value of 1.0 corresponds to a circular cross-section. The mean value for the normal patients was 1.01 (±0.01 S.E.M.) and was 1.13 (±0.03 S.E.M.) for patients with abdominal aneurysms. There was no significant difference between the two groups ($P>0.05$). As a result, I concluded that the lumen was circular in cross-section for both groups from just below the renal arteries to the throat.

5.4. Discussion

Since aneurysm size is an important factor in rupture (Reilly and Tilson, 1989), it is important to determine which imaging modality gives the best resolution of the size of the aneurysm (Todd et al., 1989). This is probably the most important parameter for screening, but could not be adequately assessed with either of these radiological methods. Ultrasound, or CT with smaller slice intervals, would be more satisfactory (Vowden et al., 1989).

Most large aneurysms contain thrombus (Figure 5.1) as shown clearly in CT images obtained with contrast injection. In Figure 5.1a, which is near the origin of the aneurysm, the contrast fills most of the lumen. By comparison, in Figure 5.1d, only the centre of the lumen contains contrast and the rest is thrombosed. In this case, the lumen is near the centre of the aneurysm.

The aneurysm, which has a flared region from its origin to the aneurysm apex, and a tapered region from the aneurysm apex to its distal boundary is a good example of the effects of these luminal area changes on flow. The velocity will decrease as in the flared region and increase past it. In the flared region, a